REPORT 963

INVESTIGATION WITH AN INTERFEROMETER OF THE TURBULENT MIXING OF A FREE SUPERSONIC JET

By PAUL B. GOODERUM, GEORGE P. WOOD, and MAURICE J. BREVOORT

Langley Aeronautical Laboratory
Langley Air Force Base, Va.

National Advisory Committee for Aeronautics

Headquarters, 1724 F Street NW, Washington 25, D. C.

Created by act of Congress approved March 3, 1915, for the supervision and direction of the scientific study of the problems of flight (U. S. Code, title 50, sec. 15). Its membership was increased from 12 to 15 by act approved March 2, 1929, and to 17 by act approved May 25, 1948. The members are appointed by the President, and serve as such without compensation.

TECHNICAL COMMITTEES

AERODYNAMICS
POWER PLANTS FOR AIRCRAFT
AIRCRAFT CONSTRUCTION
OPERATING PROBLEMS
INDUSTRY CONSULTING

Coordination of Research Needs of Military and Civil Aviation
Preparation of Research Programs
Allocation of Problems
Prevention of Duplication
Consideration of Inventions

LANGLEY AERONAUTICAL LABORATORY, Langley Field, Va.

LEWIS FLIGHT PROPULSION LABORATORY, Cleveland Airport, Cleveland, Ohio

AMES AERONAUTICAL LABORATORY Moffett Field, Calif.

Conduct, under unified control, for all agencies, of scientific research on the fundamental problems of flight

OFFICE OF AERONAUTICAL INTELLIGENCE, Washington, D. C.

Collection, classification, compilation, and dissemination of scientific and technical information on aeronautics

REPORT 963

INVESTIGATION WITH AN INTERFEROMETER OF THE TURBULENT MIXING OF A FREE SUPERSONIC JET

By Paul B. Gooderum, George P. Wood,
and Maurice J. Brevoort

SUMMARY

The free turbulent mixing of a supersonic jet of Mach number 1.6 has been experimentally investigated. An interferometer, of which a description is given, was used for the investigation. Density and velocity distributions through the mixing zone have been obtained. It was found that there was similarity in distribution at the cross sections investigated and that, in the subsonic portion of the mixing zone, the velocity distribution fitted the theoretical distribution for incompressible flow. It was found that the rates of spread of the mixing zone both into the jet and into the ambient air were less than those of subsonic jets.

INTRODUCTION

Considerable work, both theoretical and experimental, has been done in the past on free jets. Most of the theoretical work has been based on Prandtl's concept of the "mixing length." Tollmien (reference 1) and Görtler (reference 2) treated the turbulent mixing of incompressible jets. Abramovich (reference 3) published a theory of the free subsonic jet in which effects of compressibility were included. Experimental results on velocity distribution in the mixing region and rate of spread of the mixing region both into the jet and into the surrounding air have been published by various investigators (references 4 to 8). Most of the experimental work has dealt with constant-density cases; that is, the density of the jet was the same as that of the ambient air with which it mixed, and the velocity of the jet was quite small. This report presents results of an experimental investigation of the mixing of a supersonic jet. In this jet the Mach number was 1.6 and the density was about one and one-half times the density of the ambient air. Measurements were made with an interferometer of the density variation across the mixing zone in the region near the nozzle. From the density variations the velocity variations have been calculated. A full description of the interferometer is given, together with discussions of the technique of adjusting the interferometer, the theory of fringe formation, and the method of evaluating interferograms.

SYMBOLS

a	constant
b	fringe spacing; constant
c	constant $(\sqrt{1/2\sigma^3})$
c_1	constant in Snell's law
c_2	constant of integration
c_p	specific heat of air at constant pressure
$C=\frac{\lambda_0}{L(n-1)}$	
k	Gladstone-Dale constant
l	mixing length
L	distance through test section
n	index of refraction of air of density ρ
n'	index of refraction of air of density ρ'
$p=\frac{ac_1}{V_0}$	
$q=\frac{bc_1}{V_0}$	
$S(y)$	dimensionless fringe shift, Y/b, where density is ρ'
T	static temperature of air
T_{stag}	stagnation temperature of air
u	velocity of air
u_0	velocity of air in free stream
V	velocity of light
V_0	velocity of light in vacuum
V'	velocity of light in air of density ρ'
x	coordinate
X	retardation of light beam that causes fringe shift Y
y	coordinate
Y	fringe shift
z	coordinate
λ	wavelength of light
λ_0	wavelength of light in vacuum
λ'	wavelength of light in air of density ρ'
$\xi=p+qy$	
ρ, ρ', ρ_{atm}	density of air
σ	scale factor determined by comparing experimental and theoretical velocity distributions
ϕ	angle of incidence of light ray

APPARATUS

JET

The open jet is operated by the air from a 500-cubic-foot storage tank in which the initial pressure is about 180 pounds per square inch and from which a pipe leads to a supersonic nozzle. The exit end of the nozzle is open to the atmosphere. In the pipe that runs from the tank to the nozzle is a hand-operated gate valve, an air-operated quick-opening valve, and a pressure regulator. The purpose of the pressure regulator is to reduce the pressure of the air going into the nozzle to a value that will result in the pressure of the air, as it leaves the nozzle, being atmospheric. The result is that no strong shock waves or expansion waves originate at the rim of the nozzle to adjust the jet pressure to atmospheric.

The results reported herein were obtained with a nozzle that gave a Mach number of 1.6. The nozzle was of the two-dimensional type and was constructed of steel. It

had an exit opening of 3 by 3 inches. The coordinates of the nozzle blocks were calculated by the method of characteristics. No allowance was made for the thickness of the boundary layer, and the nozzle gave the Mach number for which it was designed. A photograph of similar nozzles is shown as figure 1, together with the section for the transition from a 6-inch circular pipe to the rectangular entrance to the nozzle.

INTERFEROMETER

Introduction.—The Mach-Zehnder type of interferometer was originated by L. Mach and Zehnder for use in studying phenomena of gas dynamics. The instrument is useful in the study of gas-flow problems because it gives an instantaneous record from which can be calculated the variation of gas density throughout a flow field. It is particularly applicable to the study of high-speed gas flows, because, by using light waves, it makes unnecessary the insertion into the flow of probes or other measuring instruments that would disturb the flow. The interferometer gives quantitative results in which a rather high degree of accuracy can be obtained. It has a sufficient range of sensitivity to measure both small density changes, as in a weak Prandtl-Meyer expansion, and large density changes, as across a strong shock wave.

The interferometer was used, but not intensively, by Mach and Zehnder. It was applied to the study of subsonic aerodynamics by Zobel (reference 9). Since then it has been applied by Ladenburg and his coworkers to the study of phenomena in supersonic flow (reference 10).

The basic arrangement of the Mach-Zehnder interferometer is shown in figure 2. Light from a source S is made into a beam of parallel rays by a collimating lens system L_1. This beam falls on the splitter plate S_1 where it is split into two beams. Part of the original beam of light is reflected by the splitter plate S_1 and part is transmitted by it. The part that is transmitted goes to the mirror M_1 where it is reflected onto the splitter plate S_2. A portion of the beam is transmitted by S_2 and is not used. The other portion is reflected by S_2, passes through the lens L_2, and falls on a screen or a photographic plate P.

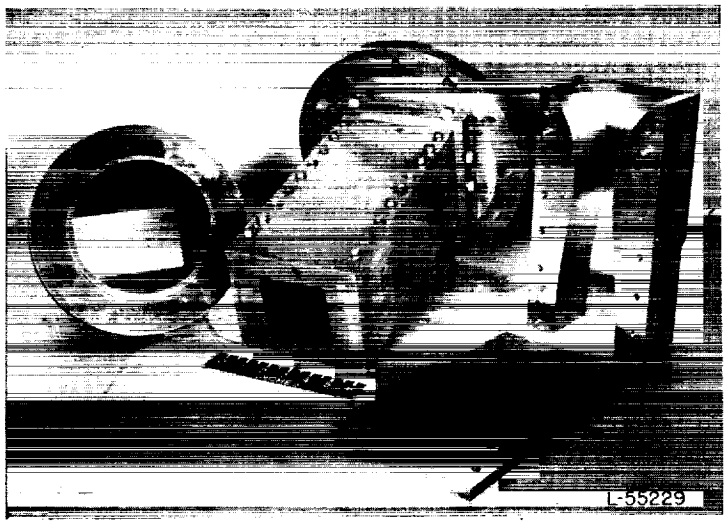

FIGURE 1.—Supersonic nozzles.

The light that was reflected by S_1 likewise goes to a totally reflecting mirror M_2 from which it is reflected onto the splitter plate S_2. At S_2 a part of the beam is reflected and is not used, and the remainder is transmitted, passes through the lens L_2, and falls on the screen or the photographic plate P. This arrangement fulfills one of the necessary conditions for the interference of the waves in two beams of light; that is, that the two beams originate in the same light source. From a practical standpoint the arrangement also permits the condition to be met that the two beams be widely enough separated in space that the disturbance to be studied can be introduced into one of the beams without disturbing the other. The disturbance, or the "test section," can, of course, be located anywhere in either of the two beams. In the apparatus described in this report, the test section was situated midway between the mirror M_2 and the splitter plate S_2.

Theory of ideal fringe formation.—The two beams of light that reach the photographic plate P appear to come from separate sources that are situated somewhere to the left of the mirror M_2. By proper orientation of the two splitter plates and the two mirrors, the two beams of light can be made to appear to cross each other, as is shown in figure 3. If, for the moment, it is assumed that each beam is composed of strictly parallel and monochromatic rays, then the wave fronts can be represented by equally spaced straight lines perpendicular to the direction of propagation, as is also shown in figure 3. Here the straight lines represent the crests of the waves. Midway between two successive crests are the troughs of the waves. Where two lines intersect, two crests occupy the same position in space, reinforce each other, and cause an increase in the amplitude of vibration and an increase in the intensity of the light. Where a line intersects a point that is midway between two adjacent lines of the other beam, a crest and a trough interfere destructively, so that a decrease in the amplitude of motion and a decrease in the intensity of the light results. The plate P will therefore be crossed by parallel, horizontal (in this case) lines of alternately weak and strong intensity. These lines are the interference fringes. They can be oriented in any direction by proper rotation of the two splitter plates and the two mirrors about two axes: one in a plane parallel to that of the paper and one perpendicular to the plane of the paper.

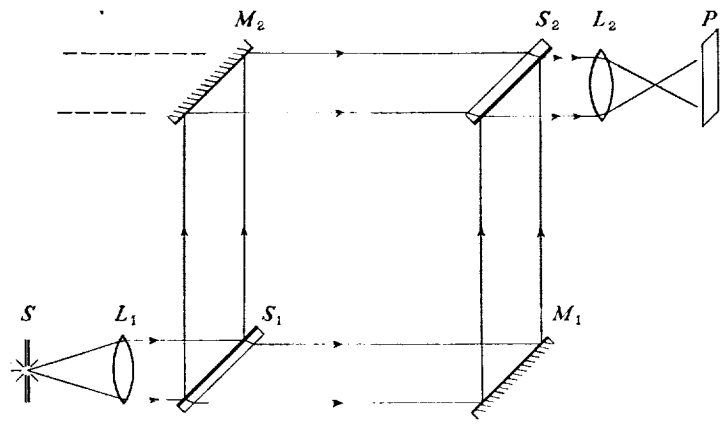

FIGURE 2.—Basic arrangement of Mach-Zehnder interferometer.

If now a disturbance is produced in the air that is in the test section and this disturbance changes the speed of the light in the beam that actually traverses the test section, then the wave fronts in that beam will be advanced or retarded, and the positions of the fringes will be shifted down or up. From the shift in the fringes the average speed of the light and, from that, the average density of the air can be calculated. The only gas-flow cases for which the density field can be evaluated are the one-dimensional case of uniform density throughout the field, the two-dimensional case of uniform densities along lines (or planes) that lie parallel to the light-beam direction of propagation, and the three-dimensional case of axially symmetric densities, such as the flow field about bodies of revolution at zero angle of attack.

Theory of practical fringe formation.—So far it has been assumed that the light is strictly monochromatic and is a beam of parallel rays. But parallel light can be obtained only from a truly point source. Because in practice neither monochromatic light nor a point source is used (with available means of approximating these to a very high degree, the intensity of the light would be too small), neither condition is actually met. As has been pointed out before (reference 10), the complete theory of fringe formation for the actual case has not yet been given. Schardin, however, has shown (reference 11) that the following is the case. With a point source and a strictly parallel beam, fringes are formed at all points along the two axes I_1—I_1' and I_2—I_2', where the two beams overlap. (See fig. 4.) But in an actual case, in which a light source of finite extent is used, the lines I_1—I_1' and I_2—I_2' become very numerous. The most distinct fringes are then formed where the various lines between I_1 and I_1' and between I_2 and I_2' intersect. The interferometer should be so adjusted, by rotation of the splitter plates, that this intersection is in the center of the test section.

For obtaining the greatest contrast between fringes, it is also necessary that the optical-path length through the interferometer be the same for the two beams. In other words, it is necessary that the optical path for the two beams be nearly the same from the time the original beam is split into two, at the splitter plate S_1, until the two are reunited at the splitter plate S_2. This condition becomes the more important the further the light departs from being monochromatic. For a given setting of the splitter plates and the mirrors, the fringes have a given spacing for each wavelength. The greater the wavelength, the greater the spacing between wave fronts and, consequently, between fringes. Thus, fringes produced by a large number of wavelengths coincide only at one point, the center of the band of fringes. On either side of this center the fringes get out of step with each other and the contrast between light and dark becomes less and less. With the optical paths equal, the center of the band of fringes, where the contract is greatest, lies at the center of the test section.

Description of interferometer.—The interferometer, with which the results presented in this report were obtained, was designed and constructed at the Langley Laboratory and is installed in the boundary layer laboratory of the Physical Research Division. The base on which the splitter plates and mirrors are mounted is a one-piece iron casting in the form of a four-leaf clover. (See figs. 5 and 6.) The assembly is supported in a vertical plane at its center by a single mount, which is attached to a framework of structural steel that is welded to a steel table. The table rests on steel plates that are bolted to the concrete floor of the second story of the building. The building houses numerous motors, compressors, and other sources of vibration. It is within 50 feet of a projectile gallery, a 500-horsepower wind tunnel, and a 1,000-horsepower wind tunnel. All of these pieces of equipment cause vibrations of considerable amplitude in the second-story floor, which is supported by columns only every 20 feet or so.

Interferometers are quite delicate instruments, as far as adjustment is concerned, and are quite subject to being thrown out of adjustment by mechanical vibrations and by temperature changes. When the present instrument was designed, it was hoped to produce an instrument that would not cause an inordinate waste of time in keeping it in adjustment. The result has been quite satisfactory. Apparently because of its symmetrical design (and probably also because cast iron has a low coefficient of thermal expansion), no effects of temperature changes on the adjustment of the interferometer have ever been noticed. Ordinarily the interferometer is enclosed in a sheet-aluminum case. Even

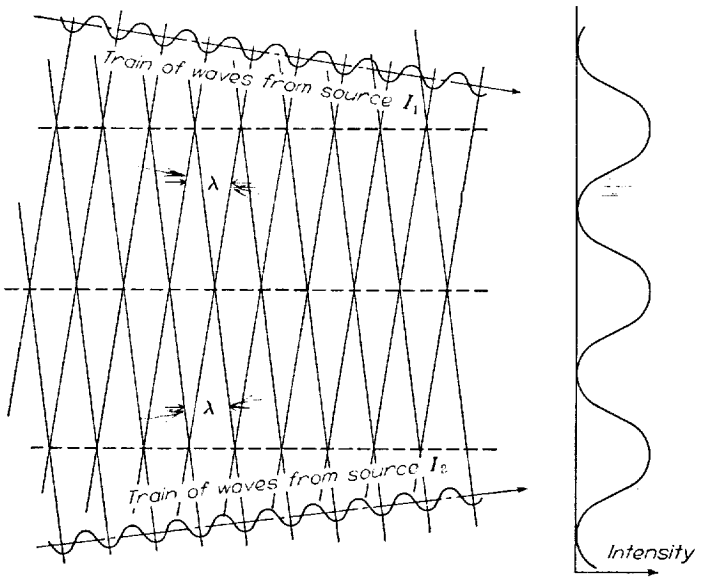

FIGURE 3.—Production of fringes with monochromatic parallel light. λ, wavelength of light.

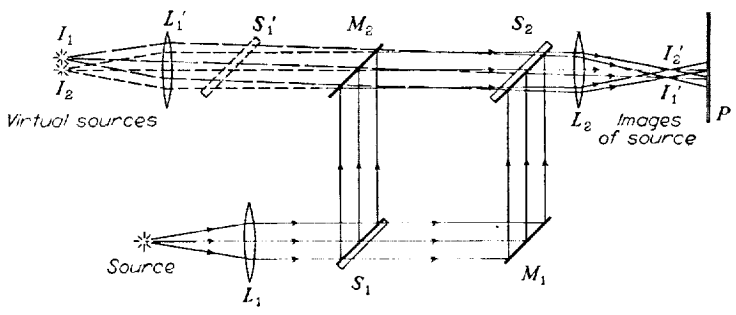

FIGURE 4.—Region in which fringes appear to be formed in Mach-Zehnder interferometer

when it is used with one side of the case removed and the temperature in the room is changed by opening the windows, or when the operators stand close to the interferometer, no change in the fringes is noticed.

In an effort to keep the interferometer in adjustment despite vibrations, it was at first suspended from a framework by springs that gave the system a natural frequency of about 1 cycle per second. It was soon found, when studying the boundary layer on a flat plate, that the beam of light could not be kept lined parallel with the flat plate. Moreover, at that time the glass plates and mirrors were supported at four points, and they could not be clamped very tightly without causing strains in the glass and distortion of the fringes. As a result, the interferometer would not stay long in adjustment, despite the fact that it was suspended by springs. Accordingly, the supports of the plates and mirrors were changed to the three-point type (see fig. 7) and were clamped down very tightly without distorting the fringes. The spring support was discarded and the interferometer table was placed on the floor as just described. As a result, the interferometer has stayed in adjustment for some length of time. In fact, in the past 9 months no adjustments of any kind have been made, and the interferometer has stayed in perfect adjustment.

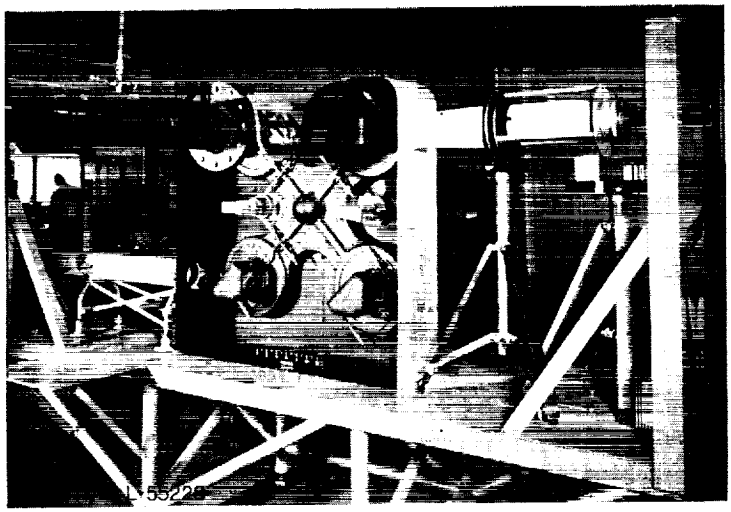

FIGURE 5.– Full view of interferometer with light source (left) and camera (right).

FIGURE 6.– Interferometer. (Splitter plates, lower left and upper right; mirrors, upper left and lower right.)

Each of the two plates and two mirrors is rotatable about two axes: one in a plane parallel to that of the interferometer base (fig. 6) and the other perpendicular to the plane of the interferometer base. For rotation about the first of these axes, the mirror holder is mounted in journal bearings. (See fig. 7.) These bearings are clamped tight, just short of binding. A lever is attached to the axle. The ends of micrometers press against the lever. Rotation of the plate or mirror is effected by advancing one micrometer while retracting the other. When the proper position is reached, both micrometers are screwed very tightly against the lever. For rotation about the other axis, the plate or mirror housing rotates on ball bearings. Again a lever is moved by means of two micrometers. (The micrometers provide an economical method of obtaining precision screw treads. The scales on the micrometers are not used.)

For adjustment of the white-light fringes—that is, for adjusting the difference in optical-path length of the two beams, where optical-path length is defined as the integral

FIGURE 7.—Interferometer mirror mount.

of the product of index of refraction and the differential of geometric path length—means were provided whereby the entire housing of mirror M_1 could be translated in a direction perpendicular to the plane of the mirror. The ways on which the housing moved were found, however, to be not sufficiently smooth, and when the mirror was moved, the plane of the mirror changed and thus the orientation of the fringes changed. The screw was also found to be too coarse; therefore, for easier adjustment of the white-light fringes, a compensating plate was installed in each beam (C_1 and C_2, fig. 8). Each plate is rotatable about two mutually perpendicular horizontal axes. One plate is placed in a horizontal position, and the white-light fringes are adjusted by rotating the other plate. The fact that the path in glass may be different for the two beams does not matter, because the light is too nearly monochromatic for dispersion to have an appreciable effect.

The splitter plates and the mirrors are 4 inches square and ½ inch thick. The plates are polished flat on each side to a tolerance of ⅒ wavelength. The angle of the wedge formed by the two sides of a plate does not exceed 2 seconds of arc. One side of each plate is coated with zinc sulphide for increased reflection. Use of this coating is a departure from the conventional method. This coating has the advantage over the conventional one, which is a thin coating of silver or aluminum, in that no light is absorbed by the coating. The ideal coating would transmit 50 percent of the light and reflect 50 percent. Since each beam is transmitted once and reflected once at splitter plates, the net result would be two beams going into the camera, each of which had 25 percent of the intensity of the original beam. For the zinc sulphide coating that was used, approximately 40 percent is reflected and 60 percent transmitted. This is satisfactory, however, because each beam into the camera then has 24 percent of the original intensity (neglecting losses at the mirrors).

The two mirrors are flat to a tolerance of ⅒ wavelength and are front surfaced with rhodium. Because of the low reflectance of rhodium (about 75 percent), it is expected that aluminum would be more satisfactory.

Description of light source and camera.—A satisfactory light source for application of interferometry to the study of flow phenomena must provide nearly monochromatic light in a nearly parallel beam. An additional requirement for taking interferograms of high-speed flow is that the duration of the light be sufficiently short. For taking interferograms that are free from blurring of phenomena in an open, or free, supersonic jet, exposure times of the order of 3 microseconds or less must be used. (Inherent in free supersonic jets are high-frequency vibrations.) Because meeting each of the requirements of being monochromatic, parallel, and of short duration tends to reduce the intensity, one must add the fourth and obvious requirement of sufficient intensity.

The light-source problem has been solved by the same general method that was used by the Princeton group (reference 10); that is, by use of a high-voltage magnesium spark and a monochromator. A diagram of the complete light-source optical system is shown in figure 8. The two electrodes are magnesium rods of ¼-inch diameter with rounded tips approximately 1 inch apart. Each magnesium rod is held in a concentric hollow brass rod. A press fit is used for

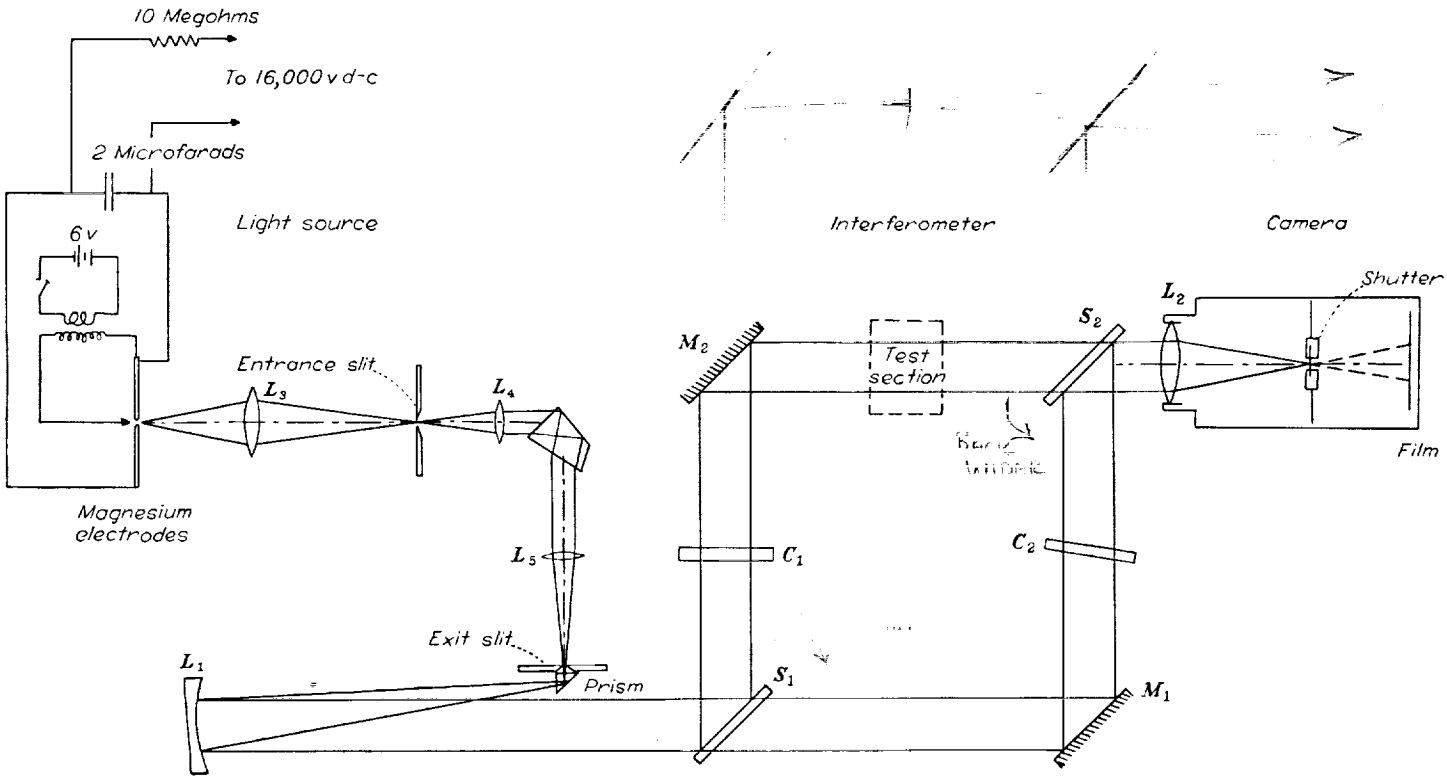

FIGURE 8.—Complete optical diagram of interferometer used in this investigation.

mechanical strength, and where the magnesium rod enters the brass rod, a weld is made. Each brass rod is soldered to a thin copper sheet, which extends for about an inch and is then soldered to a terminal on each of two condensers. Each of the two condensers, which are thus connected in parallel, is a 15,000-volt pyranol condenser and has, according to the manufacturer's specifications, a capacitance of 1.0 microfarad and an inductance of 0.5 microhenry. The condensers are charged, through a 10 megohm isolating resistor, to 16,000 volts. The discharge is initiated by means of a tickler spark between one of the magnesium electrodes and an auxiliary magnesium electrode placed between the other two and slightly to one side. The tickler spark is produced by the potential across the secondary of an automobile ignition coil that occurs when the 6-volt circuit through the primary is broken. This arrangement gives satisfactory control over the main discharge and facilitates synchronizing it with the opening of the camera shutter. The duration of the light from the main discharge was measured with a rotating-mirror apparatus and was found to be approximately 3 microseconds.

The monochromator was constructed from a Bausch and Lomb "Simplified Constant Deviation Prism Type" Laboratory Spectrometer. The collimator objective, of aperture $f/8$, and the entrance slit of the original spectrometer were removed and were replaced by a system of greater aperture that was constructed from available lenses. The lens L_3 (fig. 8) is an $f/1.6$ Kodak Anastigmat of 50-millimeter focal length. This lens focuses the light from the spark discharge on the adjustable entrance slit. (No pinhole is used at the spark.) The light is then made into a parallel beam by the lens L_4, which is an $f/2.3$ Bausch and Lomb Baltar of 2-inch focal length. The parallel beam then goes through the constant-deviation prism of the Pellin-Broca type. The beam is then focused on the adjustable exit slit by the lens L_5, which is an $f/8$ lens of 6-inch focal length and is the original lens furnished with the spectrometer. The exit slit is at the focus of the mirror L_1. The light from the slit is turned at right angles by a small prism, which is placed slightly off the axis of L_1. The mirror L_1 is a parabolic mirror of 4-inch diameter and 36-inch focal length and is front-surfaced with chrome aluminum.

It is realized that considerably more light could be obtained from the system if the f-numbers of the various lenses and the mirror were properly matched, in order that the image of the entrance slit, which falls on the exit slit, would be more nearly the same size as the entrance and the exit slits. The system as used at present, however, works satisfactorily, and therefore no changes in it are contemplated.

The light from the green triplet of magnesium is used, which has wavelengths of 5,167, 5,173, and 5,184 angstrom units. Of course, at the high exciting voltage that is used, the light does not consist only of these three wavelengths but is nearly a continuous spectrum. It was found that the light from this region produced much more satisfactory interference fringes than that from any other region of the spectrum of a high-voltage magnesium spark. (The Princeton group reported (reference 10) that they obtained best results by using the blue line at 4,481 angstroms.) The monochromator was set at 5,170 angstroms, and the slits were set at a width of 0.3 millimeter. A band about 30 angstroms wide was passed by the exit slit, and about 180 usable fringes were obtained. It was found that the appearance, or contrast, of the fringes could be improved by reducing the length of the exit slit to $\frac{3}{32}$ inch.

The fringes were photographed with an Eastman Anastigmat aerial camera lens L_2 of 13.5-inch focal length and $f/3.5$ aperture. Kodak Linagraph Ortho film was used. The Linagraph Ortho is a very fast orthochromatic film of moderate contrast and high resolving power and is designed for photographing high-speed transient phenomena on green-fluorescing cathode-ray screens. Negatives of about 1½-inch diameter were taken. (Inasmuch as the film was used in the 35-mm size, a portion of the light did not hit the film. Since the interferograms shown in the present report were taken, the film has been changed to the 70-mm size.) The moderate grain size of the film permitted enlargements of sixteen or more times the diameter of the negative, or seven or more times actual size.

A Kodak Supermatic shutter was placed at the focus of the camera lens. The shutter was set at $\frac{1}{50}$ second and was synchronized with the light-source spark. For convenience in moving the film, a slightly modified Argus C–3 camera, with the lens removed, was used as a film holder.

The procedure that was followed for each interferogram of the flow was to take first an interferogram with no flow, then one with a transparent ruler in the test section for establishing the scale, then one with flow, then a final one without flow. The film was developed in Kodak D–72 for the exceptionally long time of 14 minutes at 68° F.

Adjustment of the interferometer.—When the interferometer is first set up, a number of adjustments must be made in order to obtain fringes and to orient them properly. Most of the adjustment procedure that was used is a more-or-less standard procedure, but part is original.

The first step in the initial adjustment of the interferometer is to make the reflecting surfaces of the two splitter plates and the two mirrors nearly parallel. This is done by making the two mirrors as nearly parallel as possible by eye, and then leaving them there, because it is possible to produce all fringe orientations by adjustment of the splitter plates alone (except for adjustment for white-light fringes which is made with the compensating plates). Then the plates are set nearly parallel to the mirrors by simple inspection. A small light source is placed 15 feet or more away from the interferometer, and the light is directed at plate S_1. Two sets of cross hairs are set up, one near the light source and the other near plate S_1. Two screens are set up on the opposite side of the interferometer in such positions that a lens placed after plate S_2 focuses one set of cross hairs on one screen and the other set on the other screen. Each set of cross hairs produces two images on one screen. One image is produced by the light that is transmitted through the lower part of the interferometer, and the other image by the light that goes through the upper part. The splitter plates are then so adjusted that the two images of one set

of cross hairs coincide, or merge into a single image. This procedure is repeated for the other set of cross hairs. As the adjustments for the two sets of images are not independent, they must be continued until the images of both sets of cross hairs appear to be single. The light source is now replaced by a monochromatic light source. This light source should be sufficiently close to being monochromatic so that many hundreds of fringes can be produced. The reason for this is that at this stage of the adjustment the two optical paths through the interferometer may be considerably different. If such is the case, and a light source that would give relatively few fringes is used, then the fringes cannot be found because their apparent location would be above or below the test section and out of the light beam. A satisfactory light source is a sodium-arc lamp or a General Electric B–H6 mercury lamp operated at an undervoltage of about 60 volts. The lens in the beam emergent from the interferometer is replaced by a telescope placed some 15 feet beyond the interferometer. Interference fringes generally can then be brought into focus at some point between the light source and the telescope. If they cannot be found, either the elimination of double cross-hair images has not been sufficiently achieved or the difference in optical-path length is too great. Inspection of each cross-hair image (on the screens) with a magnifying glass will usually reveal that the elimination of doubling has not been completely effected.

Once the fringes have been located, the monochromator is set up. A B–H6 mercury lamp is placed at the entrance to the monochromator. The slits are narrowed to about 0.3 millimeter and the prism set to pass the 5,460-angstrom line. The next adjustment is to tilt the fringes into the desired orientation, say a horizontal position, by rotating a splitter plate.

The next two adjustments are to move the fringes into the test section and to adjust them to the desired width or spacing. These two adjustments are made simultaneously by alternate rotation of the two splitter plates and by observing through the telescope the location and the spacing of the fringes. This adjustment is not difficult. For example, suppose the fringes are located between S_2 and the telescope and are too narrow. The first step is to determine which of the two beams goes through which path in the interferometer. This is determined by focusing the telescope on the light source and blocking off one of the paths. It is desired to have the beams cross in the test section midway between M_2 and S_2. If the slope of the beam that passes through the test section is positive with respect to the slope of the other beam, as shown in figure 4, then plate S_2 is rotated counterclockwise to bring the fringes back almost to the test section. This adjustment may make the fringes too broad. Then S_1 is rotated clockwise to move the fringes the rest of the way to the test section and at the same time to narrow them.

The next adjustment is to make the two optical-path lengths through the interferometer equal. With the fringes in focus in or near the test section, the slits are opened until the fringes visible in the telescope become faint. By rotating a compensating plate, the fringes are caused to appear to pass vertically through the test section until they disappear. The position of the compensating plate is noted, and the plate is rotated in the opposite direction until the fringes with the greatest contrast have passed through the test section and the fringes again disappear. The compensating plate is then positioned halfway between the two positions where the fringes disappeared. The interferometer is then nearly in adjustment for white-light fringes. Either the monochromator is removed and a source of white light is used, or the white light is placed just ahead of the first splitter plate without disturbing the monochromator. (A convenient point source is the zirconium-arc light.) Then a slight adjustment of a compensating plate will bring the white-light fringes into view. If the disturbance of which an interferogram is to be taken contains a region in which there is a density gradient of considerable magnitude, such as a boundary layer, the fringes will be crowded together in that region, and distinguishing individual fringes may be difficult. It is advisable to place the white-light fringes in such a position that they will move, when the disturbance is produced, into the region of density gradient and thereby provide the fringes of greatest contrast in that region.

The final adjustment is to remove what might be called "twist" from the two beams. For horizontal fringes the two splitter plates have been rotated about horizontal axes and the two images of the light source, as seen in the telescope, lie one above the other. It may be, however, that the two beams do not lie in the same vertical plane. If they do not, sharp fringes can be observed only when the source is a line of zero width (and is also vertical, for horizontal fringes). As it is necessary that the light source have a finite width, in order to give enough light, then the fringes will appear considerably blurred unless the rotation of the plates is corrected in order that the two beams lie in the same vertical plane. In order to check this, the telescope is removed and the eye placed in the emergent beam some distance away from the interferometer. The fringes may then appear to be cocked at an angle to the horizontal. If so, then as one walks toward the interferometer the fringes will slowly rotate back to the horizontal position which they had when viewed with the telescope focused on the test section. By alternately rotating the two plates about their nonhorizontal axes, the two beams can be swung until they both lie in the same vertical plane and the fringes appear horizontal when viewed from both a close and a far position.

When all these adjustments have been made, the following will be true:

(a) The fringes are centered in the test section.
(b) The fringes have the desired orientation.
(c) The fringes have the desired spacing.
(d) The white-light fringes are in the correct location in a vertical cross section through the test section.
(e) The two beams lie in a single plane.

EVALUATION OF DENSITY FIELDS

The theory of the evaluation of interferograms of one- and two-dimensional flow fields given here is no different

881764—50 —2

from that given elsewhere. (See reference 11.) The theory is repeated here for the sake of convenience. The method of measuring fringe shifts is believed to be somewhat different.

The theory of the formation of the fringes has been discussed in a previous section. The production of fringe shifts is illustrated in figure 9. Consider that when no disturbance is present both beams travel in air of density ρ and refractive index n. The value of the refractive index is a function of the density of the air, for a given wave length of light, according to the Lorentz-Lorenz relation

$$\frac{n^2-1}{n^2+2} \propto \rho$$

or

$$\frac{n+1}{n^2+2}(n-1) \propto \rho$$

Because n is very nearly equal to unity, the equation can be written

$$n-1=k\rho \tag{1}$$

where the constant of proportionality k is the Gladstone-Dale constant. Then

$$\frac{n-1}{\rho}=\frac{n'-1}{\rho'}$$

or

$$n'-n=(n-1)\left(\frac{\rho'}{\rho}-1\right) \tag{2}$$

Now let one of the two beams pass, for the distance L, through air of a different density ρ' and index n', and let values of density and index be constant along the length L, but let them be functions of the vertical coordinate y. Then the wave fronts will be distorted, as in figure 9. The amount of distortion or retardation X at any point is a function of the velocity of light at that point. The time for passage of light of velocity V' through a distance L is L/V'. In that same time, light of velocity V will pass through a distance $L+X$. Therefore,

$$\frac{L}{V'}=\frac{L+X}{V}$$

But, since

$$\frac{V}{V'}=\frac{\lambda}{\lambda'}$$

then

$$\frac{L}{\lambda'}=\frac{L+X}{\lambda}$$

or

$$X=\frac{L}{\lambda'}(\lambda-\lambda')$$

But, since

$$n=\frac{V_0}{V}=\frac{\lambda_0}{\lambda}$$

and

$$n'=\frac{\lambda_0}{\lambda'}$$

therefore

$$X=\frac{L}{n}(n'-n)$$

$$=L\frac{\lambda}{\lambda_0}(n'-n)$$

By similar triangles, it follows that

$$\frac{Y}{b}=\frac{X}{\lambda}=\frac{L}{\lambda_0}(n'-n)$$

Then, by use of equation (2),

$$\frac{Y}{b}=\frac{L}{\lambda_0}(n-1)\left(\frac{\rho'}{\rho}-1\right)$$

or

$$\frac{\rho'}{\rho}=\frac{Y}{b}\left(\frac{\lambda_0}{L}\frac{1}{n-1}\right)+1$$

If Y/b, the fringe shift in terms of fringe width, is designated by $S(y)$ and the quantity in parentheses is designated by C, then

$$\frac{\rho'}{\rho}=CS(y)+1 \tag{3}$$

In this equation ρ'/ρ is the density ratio between some position in the disturbance and the undisturbed air.

The technique of obtaining the values of the fringe shifts for a given cross section of the flow field is simplified by the plotting of graphs. An interferogram is taken of the undisturbed fringes. (See, for example, fig. 10.) Then interferograms of the flow field are taken. (See fig. 11.) Then enlargements to about 7 diameters are made. A

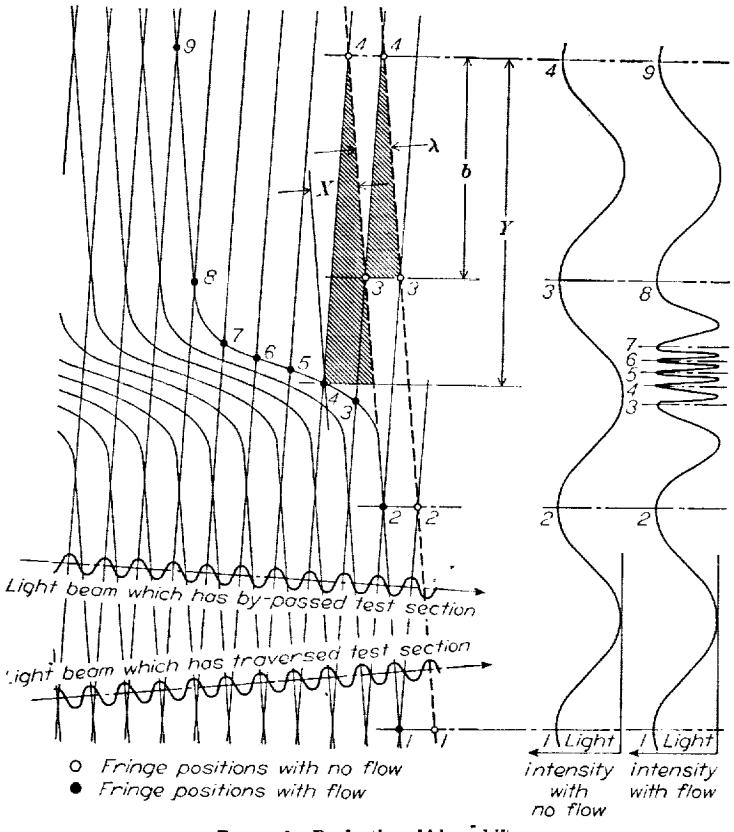

FIGURE 9.—Production of fringe shifts.

position along the horizontal axis is chosen at which the density variation is to be determined. At that position on the enlargement of the undisturbed fringe pattern, a vertical line is drawn, and the positions of the fringes are measured with a scale. (A piece of cross-sectional paper pasted on the picture is useful.) Then the fringe positions are plotted as a function of the vertical coordinate y. Such a plot is shown in figure 12. A convenient position, such as the lower edge of the nozzle opening, is chosen as the zero of the y-coordinate. This position was located on the picture in the following manner: Two small pieces of drill rod were inserted into the lower nozzle block. From their actual diameter and their measured diameter on the picture, the magnification over actual size was determined. From the known distances of these rods to the inside edge of the nozzle, the location of the edge could be found on the picture. Two small pointers placed in the camera, the shadows of which can be seen in the lower part of the interferograms, served to locate, in the pictures that did not include the nozzle end, the horizontal line that would extend to the nozzle edge. (The two pieces of drill rod were also used for checking the alinement of the light beam with the nozzle edge. They are placed on opposite sides of the center of the nozzle. If the alinement is correct, then when, on an interferogram, the proper distance is measured from each rod to give the location of the edge of the nozzle opening, the same location is obtained for both measurements.) Then, on the enlargement of the interferogram of the flow field, at the same position horizontally, the positions of the fringes were measured on a vertical scale. Then obtaining the fringe shift as a function of y was simply a matter of going to the first plot (fig. 12) with a value of y and the corresponding fringe number, reading there the undisplaced fringe number for the same value of y, and subtracting. For example, suppose that fringe number 20 lay at $y=17$ in the flow interferogram, and fringe number 8.4 lay at $y=17$ in the no-flow interferogram; then the fringe shift at $y=17$ is 11.6 fringe widths. The density ratio between the place where $y=17$ and the undisturbed air is obtained from equation (3). This procedure was carried out for each cross section through the flow field where it was decided to obtain the density distribution.

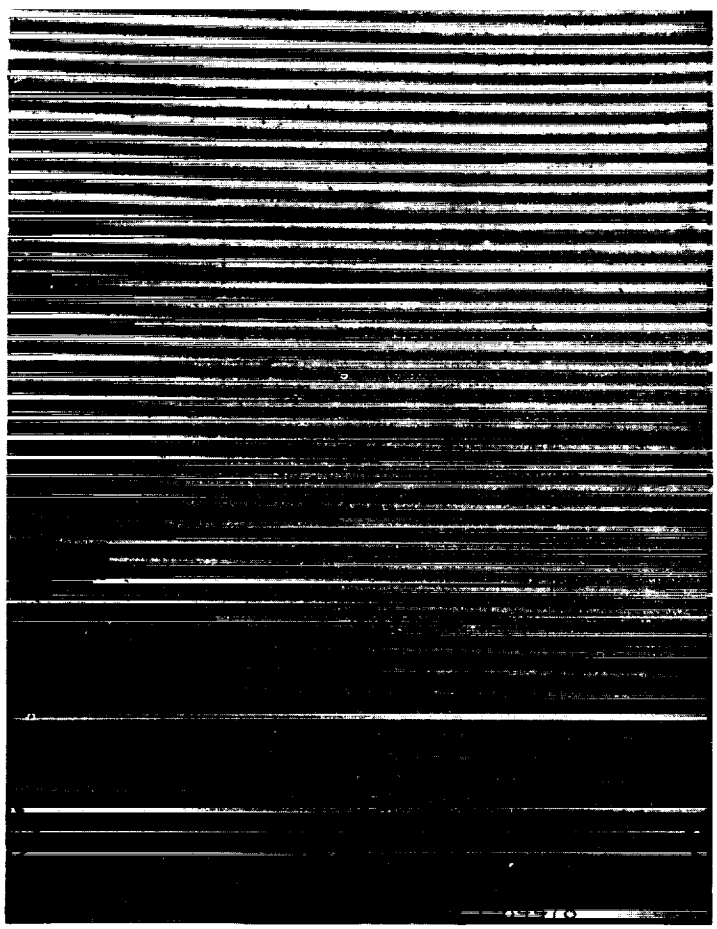

FIGURE 10. Undisturbed fringes.

The constant $C=\frac{\lambda_0}{L}\frac{1}{n-1}$ was determined for each cross section through the jet. The value of λ_0 was 5,170 angstroms. The value of $n-1$ was determined from equation (1). The value of ρ, the density of room air, was obtained from pressure and temperature measurements. The best critical-table value of k is 0.1167 cubic foot per slug for 5,170 angstroms. The width of the nozzle opening was 2.999 inches, and this value would be the value of L if there were no end effects. A corrected value of L was arbitrarily obtained as follows: The fringe shift was plotted against y from the undisturbed region, through the boundary layer, into the free-stream region of the jet. The area under the curve was obtained and divided by the fringe shift in the free stream. This gave a position at which the same fringe shift would occur if it took place abruptly, rather than gradually through the boundary layer. The difference between this position and the position of the edge of the nozzle was subtracted twice from the actual nozzle width to obtain the value of L used in the constant C. This method is sufficiently accurate for cross sections close to the nozzle.

EFFECT OF REFRACTION

When light passes through a medium in which the index of refraction varies in a direction that is perpendicular to the initial direction of propagation of the light, the direction of propagation is changed, or the light is refracted. In the mixing region of the jet considered herein, the density of the air varies, and consequently also the index of refraction varies. The purpose of the present section is to determine whether the refraction, or bending, of the light has a significant effect on the mixing-region density distribution obtained from interferograms.

Let y be the vertical coordinate through the mixing zone and z the horizontal coordinate in the direction of the light beam. Because the air density in the mixing region increases as y increases, the light will be refracted toward larger values of y. If ϕ represents the angle of incidence, then Snell's law states that, at any point in the medium,

$$\sin\phi=\frac{V}{c_1}$$

where V is the velocity of the light and c_1 is a constant.

See Also: Gilbert M Edelman and Marjorie H. Bright, "The specific refractivity

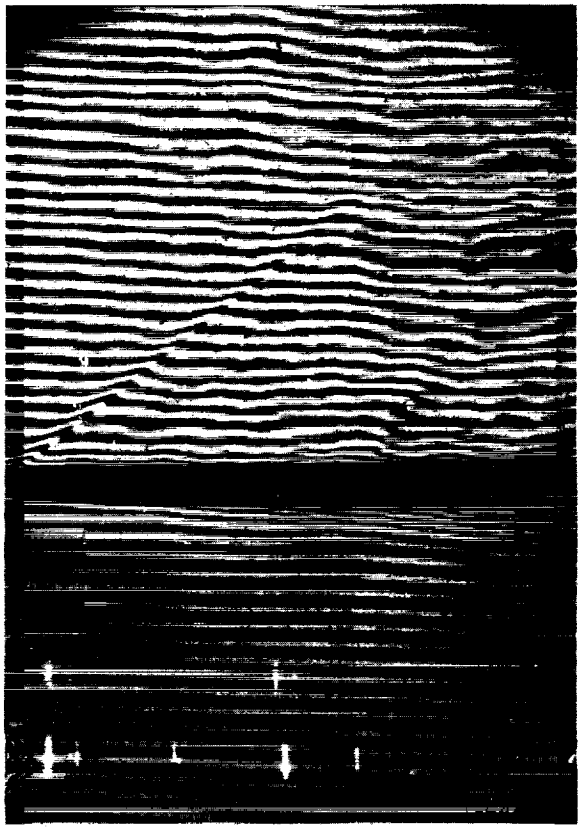

(a) 0 to 1½ inches from nozzle.

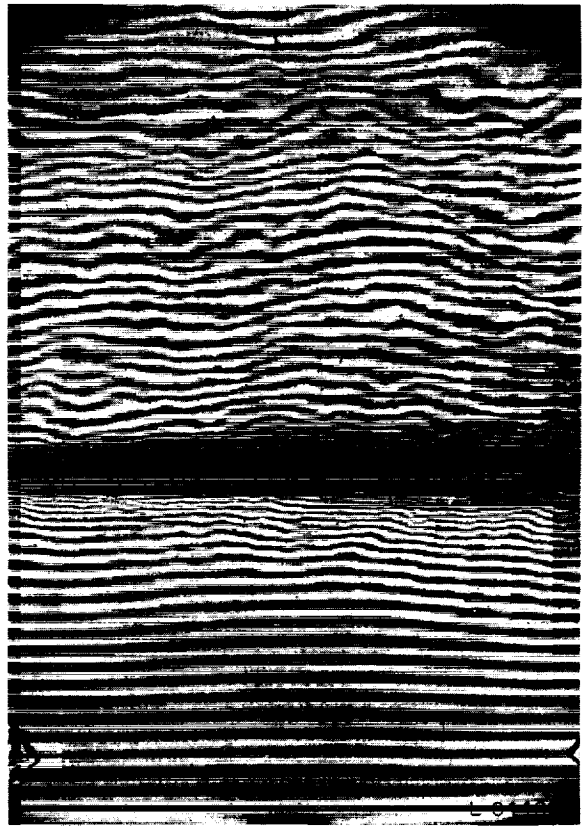

(b) 1½ to 3 inches from nozzle.

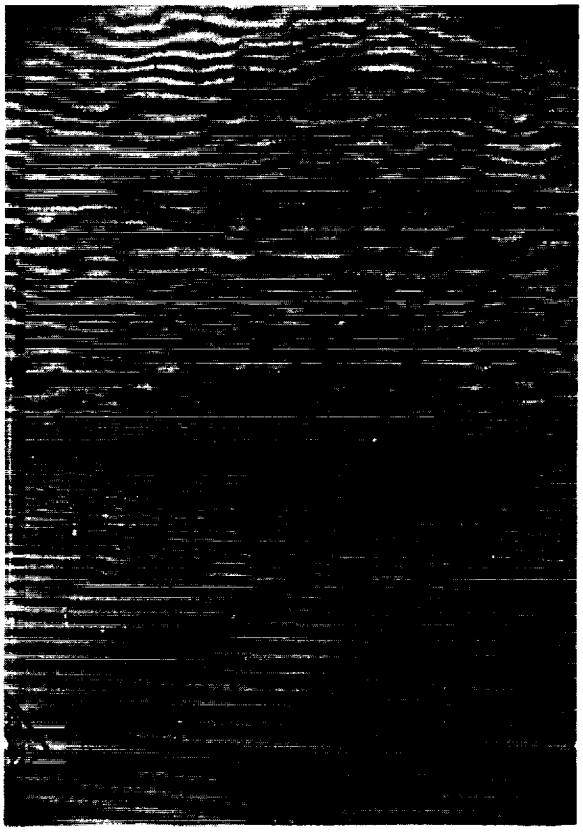

(c) 3 to 4¼ inches from nozzle.

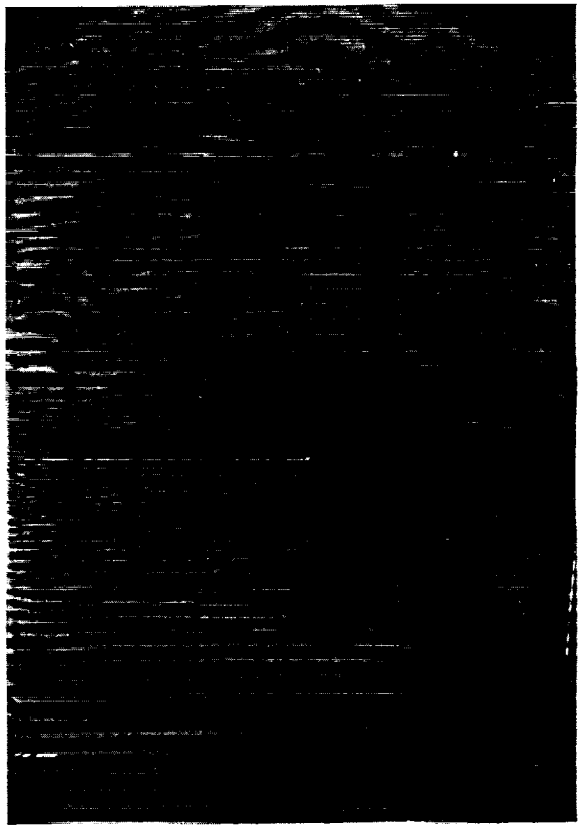

(d) 4¼ to 5¾ inches from nozzle.

FIGURE 11.—Interferogram of jet.

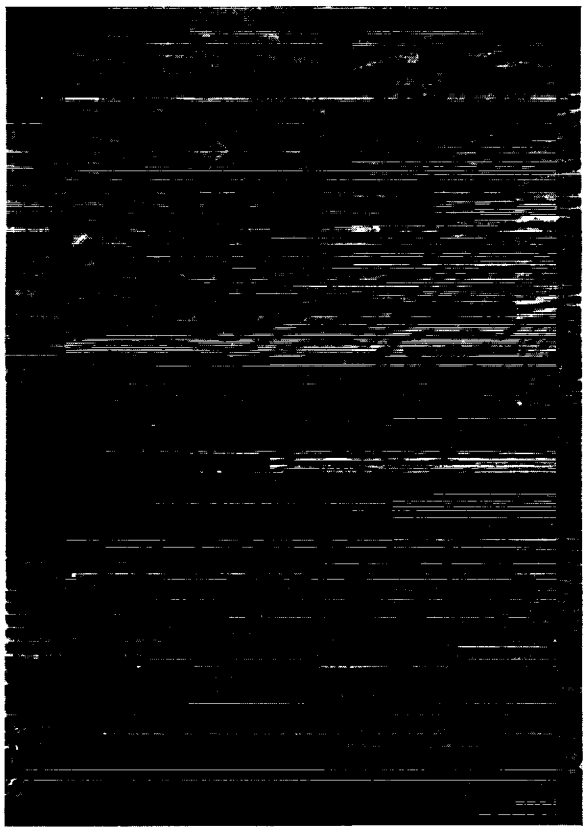

(e) 5½ to 7 inches from nozzle.

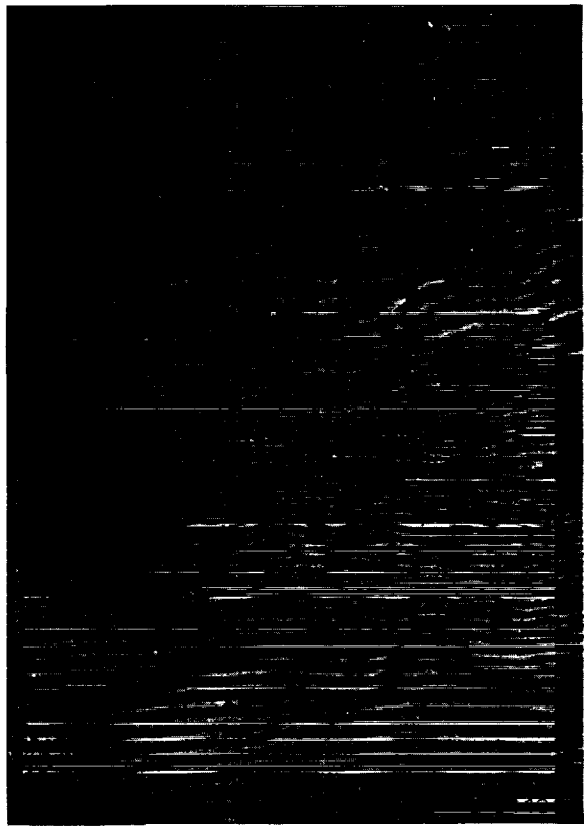

(f) 7 to 8½ inches from nozzle.

FIGURE 11.—Concluded.

Accordingly, therefore,

$$\tan\phi=\frac{\sin\phi}{\sqrt{1-\sin^2\phi}}$$

$$=\sqrt{\frac{V^2}{c_1^2-V^2}}$$

$$=\frac{dz}{dy}$$

$$\frac{dy}{dz}=\sqrt{\frac{c_1^2}{V^2}-1}$$

but

$$\frac{1}{V}=\frac{n}{V_0}$$

therefore

$$\frac{dy}{dz}=\sqrt{\left(\frac{c_1}{V_0}n\right)^2-1}$$

It is now required to solve this equation in order to find the amount by which a ray of light is deviated in the mixing region. First, it is necessary to express n as a function of y. In a subsequent section, the density distribution through the mixing region is obtained. For the present purpose this distribution is approximated by a linear variation that fits the actual variation over a large portion of the mixing region. The density of the air at the outside of the mixing zone is taken as 0.0024 slug per cubic foot and at the inside edge of the mixing region as 1.5 times as great, or 0.0036 slug per cubic foot. The effect of refraction is greatest at the place where the density gradient is the greatest. This occurs at the cross section that is closest to the nozzle. For the present investigation that cross section is 2 inches from the nozzle. The actual width of the mixing zone there is about 0.33 inch. The assumption is made of a linear density gradient equal to the average gradient across the mixing region. The assumed density variation, then, is given by the equation

$$\rho=0.0024+0.0036y$$

and the index variation is, by use of equation (1) and the given value for k,

$$n=1.00028+0.00042y$$

or

$$n=a+by$$

The differential equation then becomes

$$dz=\frac{dy}{\sqrt{\left(\frac{c_1}{V_0}a+\frac{c_1}{V_0}by\right)^2-1}}$$

By substitution of

$$p=\frac{ac_1}{V_0}$$

$$q=\frac{bc_1}{V_0}$$

and

$$\xi=p+qy$$

then

$$dz=\frac{d\xi}{q\sqrt{\xi^2-1}}$$

On integration,

$$q(z+c_2)=\log_e\left(\xi+\sqrt{\xi^2-1}\right)$$

For evaluation of the integration constant c_2, at $z=y=0$

$$qc_2=\log_e\left[\frac{c_1}{V_0}a+\sqrt{\left(\frac{c_1}{V_0}a\right)^2-1}\right]$$

But at $z=y=0$,

$$c_1=V_{(y=0)}=\frac{V_0}{n_{(y=0)}}=\frac{V_0}{a}$$

Therefore

$$qc_2=\log_e 1=0$$

and

$$c_2=0$$

Therefore

$$\xi=1+\frac{b}{a}y$$

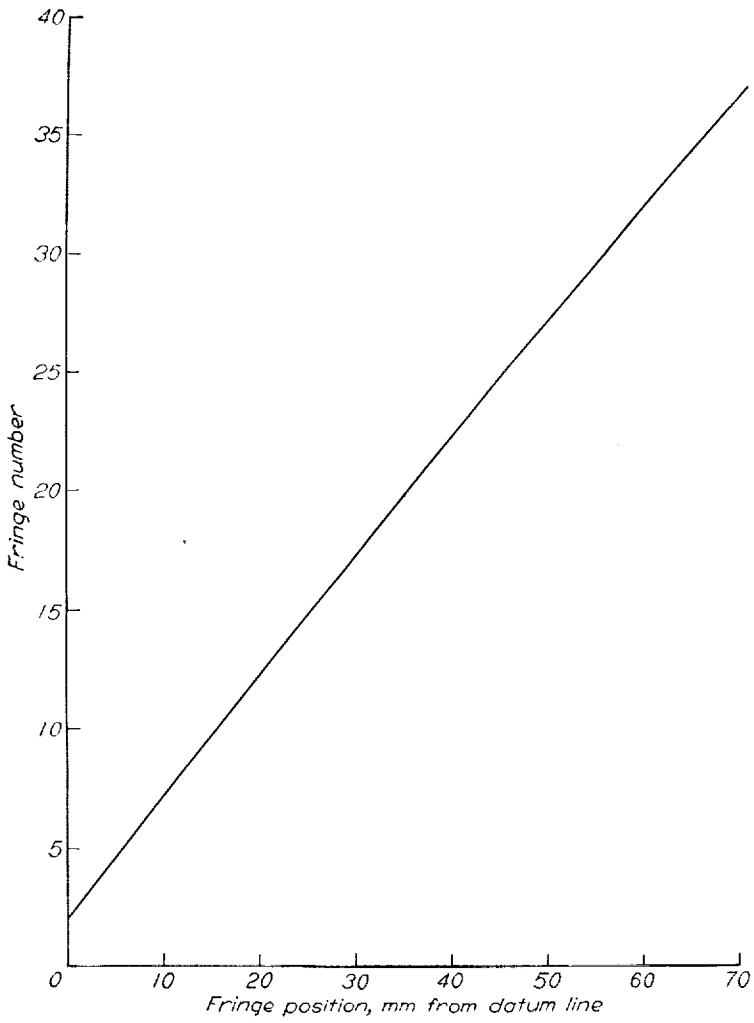

FIGURE 12.—Location of undisturbed fringes.

and

$$\frac{b}{a}z=\log_e\left[1+\frac{b}{a}y+\sqrt{\left(1+\frac{b}{a}y\right)^2-1}\right]$$

or

$$e^{\frac{b}{a}z}+e^{-\frac{b}{a}z}=2\left(1+\frac{b}{a}y\right)$$

The path of a ray, therefore, through a medium of linear density gradient is a catenary. Because a is very nearly equal to unity, the equation can be simplified to

$$e^{bz}+e^{-bz}=2(1+by)$$

or, by use of the series expansion, to

$$y\approx\frac{1}{2}bz^2$$

The deviation of a ray on passing through the 3 inches of the mixing region, from $z=0$ to $z=3$, is

$$y=\frac{1}{2}\times0.00042\times9$$

$$=0.0019 \text{ inch}$$

The index of refraction at $y=0$ is

$$n=1.00028$$

and at $y=0.0019$ is

$$n=1.0002808$$

The important quantity, though, is $n-1$. The light ray emerges from the mixing region at a place where $n-1$ differs by less than 1 percent from its value at the place where the ray entered the mixing region. For the jet under discussion, therefore, the effect of refraction is negligible.

RESULTS

INTERFEROGRAMS

For obtaining interferograms of the mixing region of the free jet of Mach number 1.6, the interferometer was so adjusted that straight, horizontal interference fringes were produced when there was no air flow, as is shown in figure 10.

Figure 13 shows the portion of the jet of which interferograms were taken for the present investigation. This portion was the bottom part of the horizontal jet for the first 10 inches from the nozzle. The 10-inch length was covered by taking a series of seven interferograms, each of which covered a portion of the jet and its mixing region that was about 2½ inches high and about 1½ inches wide. Only the first six of these interferograms were used in obtaining the density and the velocity distributions that are given in the present report. These six interferograms covered the first 8½ inches of the mixing region. The interferograms are shown as figures 11(a) to 11(f). A composite of the six interferograms is shown as figure 14.

Three regions are distinguishable in these pictures. The lower portion of each picture, where the fringes have retained essentially the same spacing that they had with no air flow, was taken with light that passed through nearly undisturbed room air. The upper portion of each picture shows the free-stream region of the jet. The center portion of each picture is the mixing zone between the free room air and the free-stream portion of the jet.

If the irregularities in the fringes in the lower and the upper portions of the interferograms are averaged out, then the spacing of the fringes is found to remain the same as it was with no air flow. This shows that there is uniform density in each of the regions. In the mixing zone, however, the fringes are crowded together and there is a density gradient in that region. The density varies, in fact, from atmospheric outside the jet to about 1½ times atmospheric inside the jet.

As can be seen in figure 11 (a), at the end of the nozzle the boundary layer that has built up along the nozzle and that emerges from the nozzle is much thicker than the beginning of the jet mixing region. At a distance of about 2 inches downstream from the nozzle, however, this boundary layer has lost its identity and there is only the mixing zone, the undisturbed jet, and the room air. Only data taken from the region between 2 and 7½ inches downstream from the nozzle are included in the present report. In that region seven vertical cross sections were chosen, at 2, 2½, 3½, 4½, 5½, 6, and 7½ inches from the nozzle.

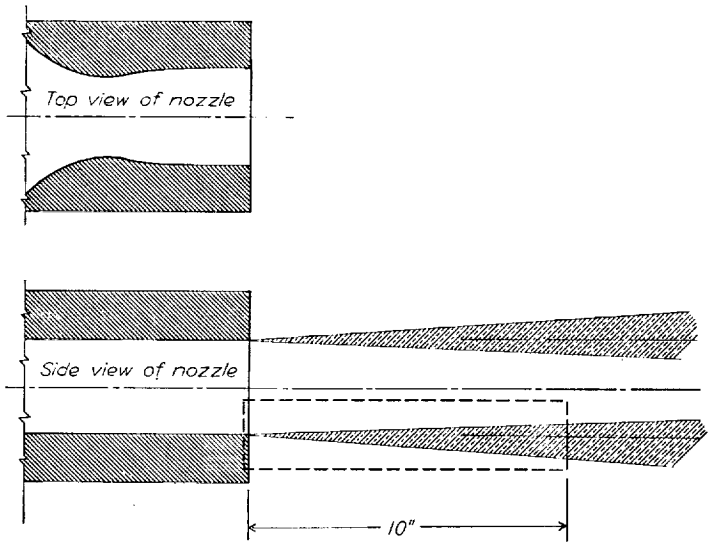

FIGURE 13.—Schematic diagram of nozzle, jet, and mixing region.

DENSITY DISTRIBUTION

The density variation along each cross section was obtained. The method of obtaining the density variation was first to measure the variation of fringe shift along each vertical cross section. This was done by the method described in the section entitled "Evaluation of Density Fields." Figure 15 shows a plot of the density variation across the mixing zone at the seven cross sections. On the vertical axis is plotted the ratio of density to atmospheric density ρ/ρ_{atm}. On the horizontal axis is plotted the nondimensional parameter $\sigma y/x$. The variables y and x are position coordinates. The y-axis is vertical. The x-axis is not quite horizontal but has been so chosen that it coincides with the line along which the density ratio is 1.1. This is the line along which the velocity is 0.5 free-stream velocity. (It has been customary in the past to place the x-axis along the 0.5-velocity-ratio contour. For the jet under discussion, this contour was at an angle of $-1¼°$ to the horizontal.) The parameter σ is an experimentally determined scale factor. Its value is obtained by comparing the experimentally determined velocity distribution with the theoretical distribution. Figure 15 shows that there is fairly good similarity in the density distributions. The lack of scatter of the experimental points at the outside portion of the mixing region is explained by the fact that atmospheric density was used as the reference in the quantity ρ/ρ_{atm} that was plotted. The scatter that occurs at the inside part of the mixing region can be attributed partly to variations in atmospheric density and partly to variations in the stagnation temperature of the jet, both of which varied from picture to picture.

VELOCITY DISTRIBUTION

From the density distributions the velocity distributions were calculated with the aid of several assumptions and

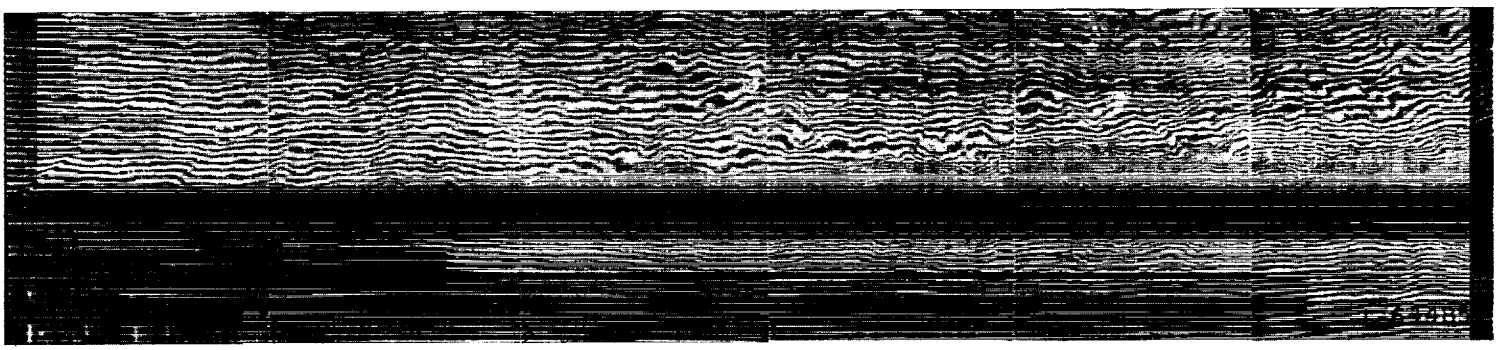

FIGURE 14.—Composite interferogram of jet, 0 to 8½ inches from nozzle.

approximations. It was assumed that the static pressure in the jet and the mixing region was the same as the pressure in the room air outside the jet. The temperature distributions through the jet were then obtained from the density distributions by the general gas law.

For the different interferograms the room-air temperature varied between 79.6° F and 80.1° F. The stagnation temperature of the jet air varied between 71.6° F and 73.6° F. (The stagnation temperature was measured with a thermocouple that was installed in the 6-inch pipe ahead of the nozzle where the air velocity was low, about 150 feet per second, and the temperature recovery factor was very nearly equal to unity.) The assumption was made that there was no heat transfer in the mixing region. The jet and the mixing region were therefore considered to be isothermal from the standpoint of stagnation temperature. For the calculations of velocity distribution, the assumption was made that the stagnation temperature in the mixing zone was the same as the temperature of the room air. Then, from the constant stagnation temperature and the static temperature distributions, the velocity distributions were calculated from the conservation-of-energy equation

$$u^2=2c_p(T_{stag}-T)$$

where u is the velocity and c_p is the specific heat at constant pressure.

Tollmien obtained (reference 1) the theoretical velocity distribution for the mixing region of an incompressible jet. His results, given in table I of reference 1, are shown in figure 16. The vertical coordinate is u/u_0, where u_0 is the free-stream velocity. The horizontal coordinate is again $\sigma y/x$. (For this figure only, the position of the x-axis has not been adjusted to coincide with the $\frac{u}{u_0}=0.5$ contour but is horizontal, at right angles to the y-axis.) Tollmien's results show that the outside edge of the mixing region of an incompressible jet is given by $\frac{\sigma y}{x}=-2.04$. Furthermore, Abramovich found (reference 3) that compressibility had no effect on the value of $\sigma y/x$ at the outside boundary of the mixing region. He treated theoretically a jet in which the stagnation temperature was the same as that of the ambient air and in which the free-stream velocity was large—up to the velocity of sound. He also treated the low-speed jet in which the stagnation temperature was different from the temperature of the ambient air. He found that compressibility effects arising from the high velocity or from the temperature difference did not affect the value of $\sigma y/x$ at the outside boundary, but that the value for both cases was -2.04. In the present report, therefore, this value has been accepted as correct.

Tollmien's results also show that the inside edge of the mixing region of an incompressible jet lies along a value $\frac{\sigma y}{x}=0.98$. Abramovich found, however, that the value of $\sigma y/x$ at the inside boundary should be affected by compressi-

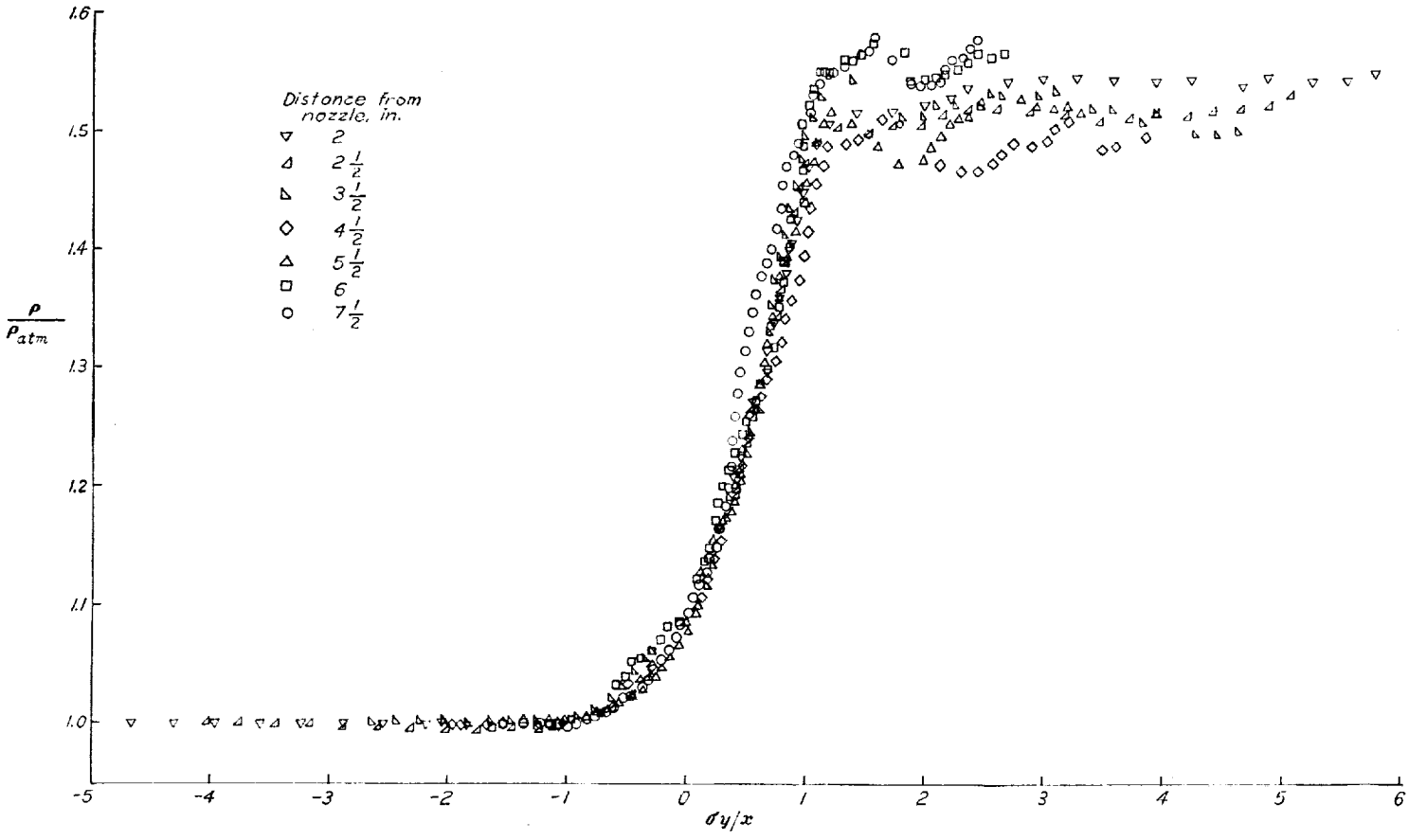

FIGURE 15.—Variation of density ratio through mixing region. $\sigma=15$.

bility considerations. His analysis, however, was not extended to supersonic velocities, and no theoretical value for $\sigma y/x$ at the inside boundary is available for supersonic flow.

The quantity σ was introduced in the theory of free jet mixing as a scale factor. (For example, see reference 1.) The theory does not give the value of σ, but its value is determined by fitting the experimentally determined velocity distribution to the theoretical velocity distribution. In the present case, the inside boundary of the mixing zone is clearly shown on the interferograms, and the angle that it makes with the free-stream direction can be measured and shown to be 3°. Because the theoretical value for $\sigma y/x$ at this boundary is not known, the value of σ cannot be determined from the measured rate of spread of the mixing zone into the jet. Furthermore, at the outer edge of the mixing zone where $\frac{\sigma y}{x}=-2.04$, the density gradient is extremely small. An interferometer is not very sensitive to such small gradients, however, and the outer edge of the mixing zone cannot, therefore, be determined accurately from the interferograms. Shadowgrams that covered an extent of 5 feet along the jet were therefore taken. On the shadowgrams the outside boundary of the mixing zone appeared to lie at approximately 6°. This angle would give a value of σ of approximately 20,

$$\sigma \approx \frac{-2.04}{-\tan 6^\circ}$$

It was felt, however, that the shadowgrams might not accurately indicate the true boundary of the mixing zone, and that the most satisfactory method of determining σ would be to choose a value that would give the best fit of the experimentally determined velocity distribution with Tollmien's theoretically determined velocity distribution over the subsonic portion of the mixing region. First, Tollmien's curve, shown in figure 16, was shifted horizontally by 0.39 in order that the 0.5 value of u/u_0 would lie at the zero value of $\sigma y/x$, as shown by the solid curve of figure 17. Then the velocity distributions that were calculated from the measured density distributions, as has been indicated, were plotted with σ taken as 15 and with the x-axis taken along the $\frac{u}{u_0}=0.5$ contour. This value of σ was chosen because it makes the data agree with Tollmien's curve between about 0.2 and 0.6 on the vertical scale. At values of u/u_0 smaller than approximately 0.2 the data are probably not very accurate. At values of u/u_0 greater than 0.625 the flow is supersonic, and it is to be expected that compressibility effects alter the velocity distribution from that of incompressible flow. In fact, figure 17 shows that the inside boundary of the mixing region of the supersonic jet is at $\frac{\sigma y}{x}=1.12$, compared with 1.37 for the incompressible jet. In the supersonic jet, therefore, the mixing region spreads into the free stream at a slower rate than in an incompressible jet.

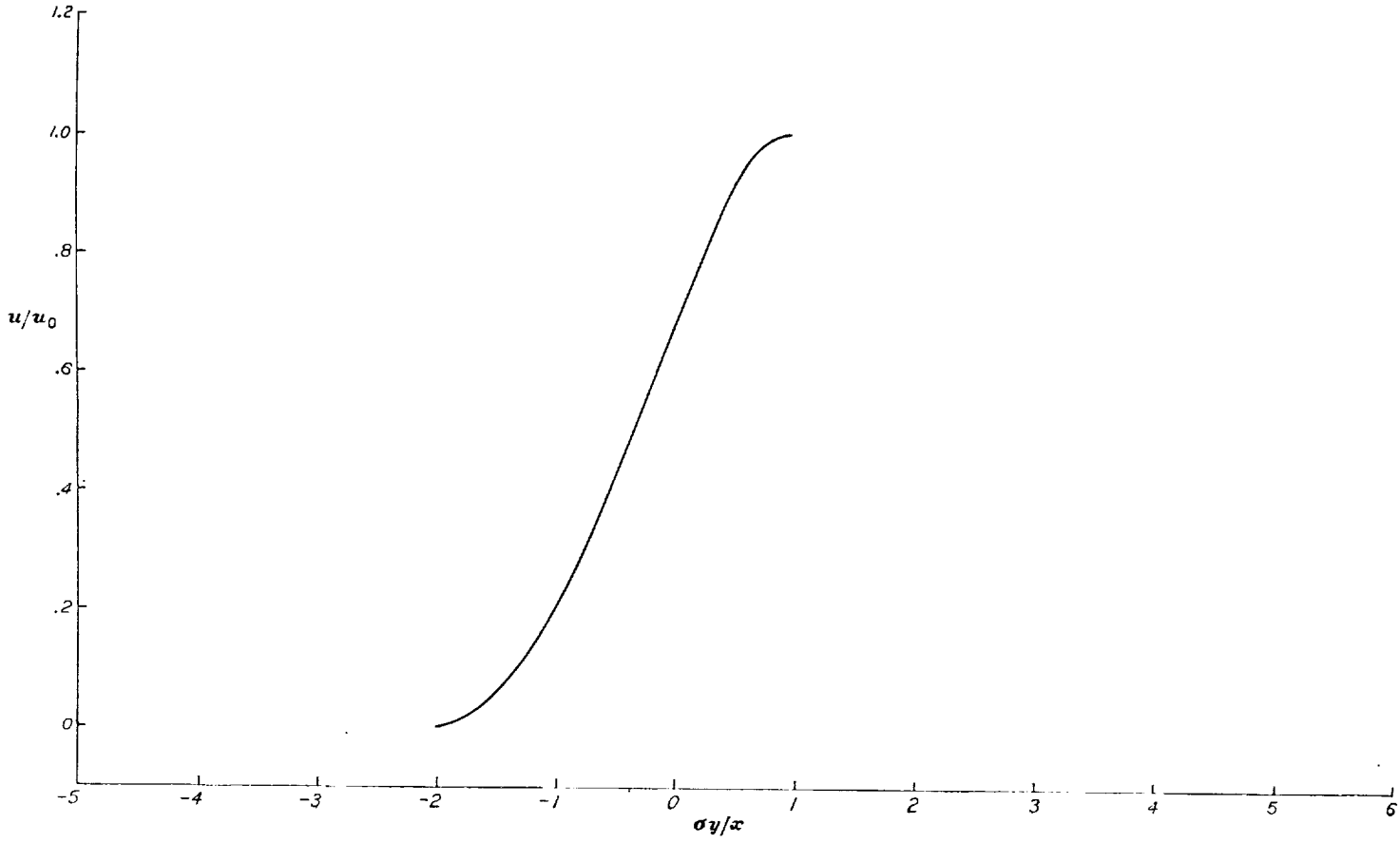

FIGURE 16.—Theoretical velocity distribution for incompressible mixing zone. (From reference 1.)

The value of σ obtained here can be compared with the values obtained by other investigators for incompressible jets. Measurements in a large jet at Göttingen (see reference 1), in which the free-stream velocity was about 100 feet per second, gave a value for σ of 11.8. Liepmann and Laufer state (reference 8) that Cordes found a value of 11.95 for σ. Liepmann and Laufer found that for their jet, which had a free-stream velocity of 59 feet per second, the value of σ was 12.0. These values are to be compared with the results of the present measurements, which give a value of 15 for σ for a jet of Mach number 1.6. Because σ is a measure of the rate of spread of the mixing region, the mixing region of the present supersonic jet spreads less rapidly than that of incompressible jets. The rate of spread of the outside boundary is $\frac{1}{15}$ that of incompressible jets. The ratio of the rates of spread of the inside boundary is even less, as is shown by the fact that in figure 17 the inside boundary lies at a smaller value of $\sigma y/x$ than the theoretical.

In the theory of the incompressible jet, it has been customary to assume that the value of the "mixing length" is constant across the mixing zone and that the value of the mixing length l is proportional to the distance from the nozzle,

$$l=cx$$

The constant of proportionality c is $\sqrt{1/2\sigma^3}$. For the subsonic jets, with $\sigma=12$, the proportionality constant c has the value of 0.017. For the supersonic jet, with $\sigma=15$, the value of c is 0.012. By the use of the hot-wire method, Liepmann and Laufer have shown that the mixing length is not constant across the mixing zone. If σ is taken, notwithstanding this fact, to be a measure of the amount of turbulence, then the present measurements show that the mixing region of a supersonic jet is less turbulent than the mixing region of a low-speed jet.

Figure 17 shows that the velocity distributions at the various cross sections are similar. The figure also shows that the flow in the mixing zone is turbulent, because the rate of spread is linear, in agreement with theory, as compared to laminar flow in which the rate of spread is a function of the Reynolds number based on the x-coordinate.

Figures 15 and 17 show density and velocity distributions, respectively, at seven cross sections. These cross sections lie between 2 and 7½ inches downstream from the nozzle. Interferograms of the region from 7½ to 10 inches downstream were also taken and density and velocity distributions were obtained. These distributions were very similar to those shown in figures 15 and 17. The distributions so obtained, however, at these distances from the nozzle are not necessarily

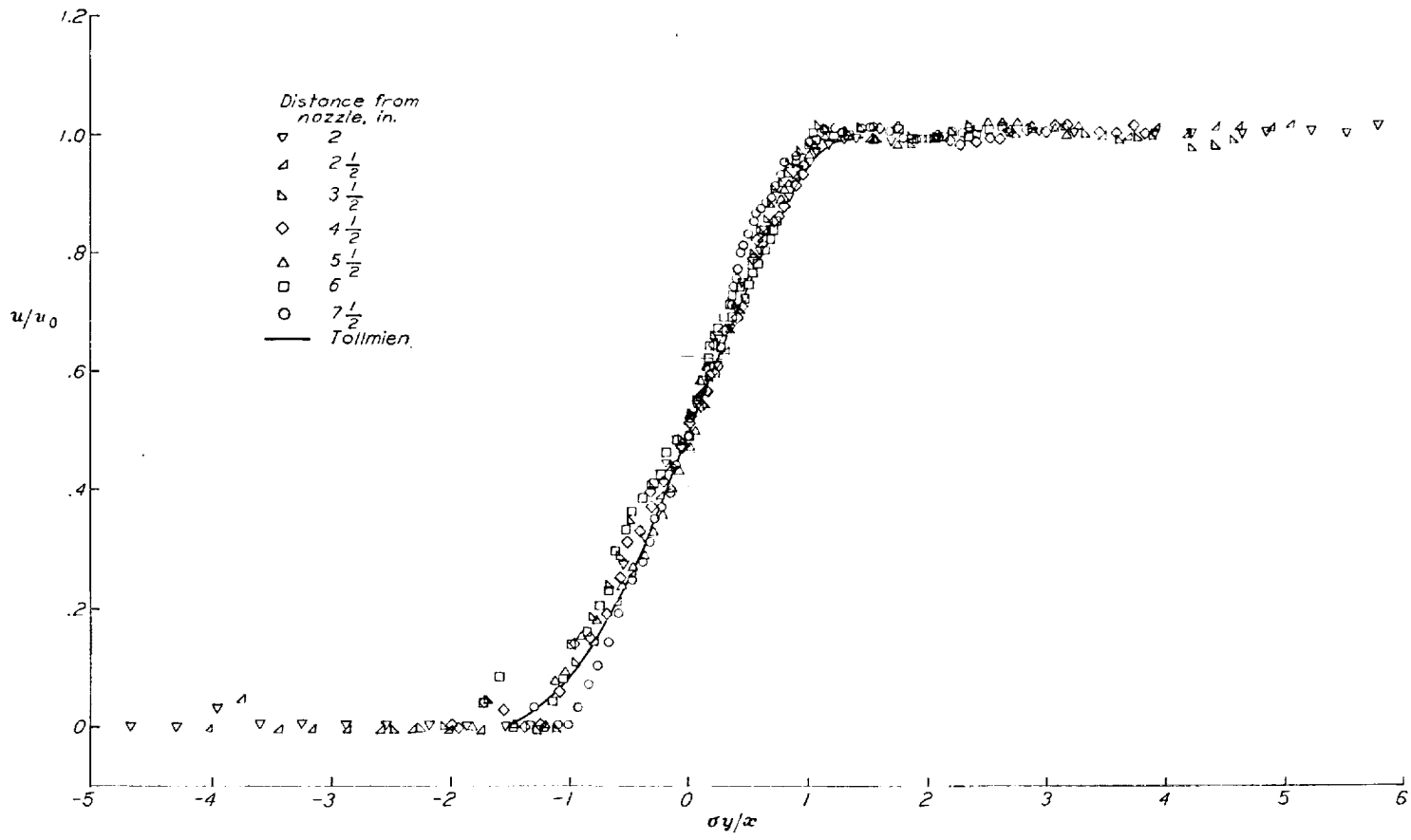

FIGURE 17.—Variation of velocity ratio through mixing region. $\sigma=15$.

accurate. At 10 inches, the path length of the light through the mixing regions on the two sides of the jet is about 3 inches. The effect of this on the results was reduced by the method described in the section entitled "Evaluation of Density Fields." When the effect is large, however, it is not certain that the method of correcting is at all accurate. For that reason no results are shown in the present report for distances greater than 7½ inches from the nozzle.

SUMMARY OF RESULTS

It has been found that, for the free supersonic jet of Mach number 1.6,

1. Density distributions through the mixing region were similar to each other at the cross sections investigated.

2. Velocity distributions through the mixing region were similar to each other at the cross sections investigated and were similar to Tollmien's theoretical velocity distribution in the subsonic portion of the mixing region.

3. The turbulence in the mixing region was less than that for incompressible jets.

4. The rates of spread of the mixing region, both into the jet and into the ambient air, were less than those of incompressible jets.

LANGLEY AERONAUTICAL LABORATORY,
NATIONAL ADVISORY COMMITTEE FOR AERONAUTICS,
LANGLEY AIR FORCE BASE, VA., *January 21, 1949.*

REFERENCES

1. Tollmien, Walter: Calculation of Turbulent Expansion Processes. NACA TM 1085, 1945.
2. Görtler, H.: Berechnung von Aufgaben der freien Turbulenz auf Grund eines neuen Näherungsansatzes. Z.f.a.M.M., Bd. 22, Nr. 5, Oct. 1942, pp. 244–254.
3. Abramovich, G. N.: The Theory of a Free Jet of a Compressible Gas. NACA TM 1058, 1944.
4. Kuethe, Arnold M.: Investigations of the Turbulent Mixing Regions Formed by Jets. Jour. Appl. Mech., vol. 2, no. 3, Sept. 1935, pp. A–87—A–95.
5. Förthmann, E.: Turbulent Jet Expansion. NACA TM 789, 1936.
6. Reichardt, H.: Laws of Free Turbulence. R.T.P. Translation No. 1752, British Ministry of Aircraft Production. (From V.D.I. Forschungsheft No. 414, May/June 1942, pp. 1–22.)
7. Corrsin, Stanley: Investigation of Flow in an Axially Symmetrical Heated Jet of Air. NACA ACR 3L23, 1943.
8. Liepmann, Hans Wolfgang, and Laufer, John: Investigations of Free Turbulent Mixing. NACA TN 1257, 1947.
9. Zobel, Th.: Development and Construction of an Interferometer for Optical Measurements of Density Fields. NACA TM 1184, 1947.
10. Ladenburg, R., Van Voorhis, C. C., and Winckler, J.: Interferometric Study of Supersonic Phenomena. Part I: A Supersonic Air Jet at 60 LB/IN² Tank Pressure. NAVORD Rep. 69–46, Bur. Ordnance, Navy Dept., April 17, 1946; Part II: The Gas Flow around Various Objects in a Free Homogeneous Supersonic Air Stream. NAVORD Rep. 93–46, Sept. 2, 1946.
11. Schardin, H.: Theory and Applications of the Mach-Zehnder Interference-Refractometer. Univ. of Texas, Defense Res. Lab., 1946.

U. S. GOVERNMENT PRINTING OFFICE: 1950

Gooderum Vol VII 1930

SYMBOLS

Symbols and formulae that occur in a single table are explained there.

- d Density.
- F Formula-weight in accordance with the printed formula.
- g As subscript, g indicates that the quantity pertains to the gas.
- H As subscript, H indicates that the quantity pertains to hydrogen, H_2.
- M Molecular weight.
- n Index of refraction referred to a vacuum.
- p Pressure.
- λ Wave-length.
- λ_μ Value of λ when the unit is $1\mu = 10^4$ Å; $\lambda_\mu = 10^{-4}\lambda_{Å}$.

SYMBOLE

Symbole und Formeln, die in einer einzelnen Tabelle vorkommen, sind dort erklärt.

- d Dichte.
- F Formelgewicht entsprechend der gedruckten Formel.
- g Als untergeschriebene Index bedeutet g, dass sich die Grösse auf ein Gas bezieht.
- H Als untergeschriebene Index bedeutet H, dass sich die Grösse auf Wasserstoff, H_2 bezieht.
- M Molekulargewicht.
- n Brechungsindex auf das Vakuum bezogen.
- p Druck.
- λ Wellenlänge.
- λ_μ Wert von λ, wenn als Einheit $1\mu = 10^4$ Å gilt; $\lambda_\mu = 10^{-4}\lambda_{Å}$.

SYMBOLES

Les symboles et formules qui se présentent dans une seule t sont expliqués à cette place.

- d Densité.
- F Formule-poids en accord avec la formule imprimée.
- g Comme souscrit, g indique que la quantité se rapporte à un
- H Comme souscrit, H indique que la quantité se rapport l'hydrogène, H_2.
- M Poids moléculaire.
- n Indice de réfraction par rapport au vide.
- p Pression.
- λ Longeur d'onde.
- λ_μ Valeur de λ lorsque l'unité est $1\mu = 10^4$ Å; $\lambda_\mu = 10^{-4}\lambda_{Å}$.

SIMBOLI

I simboli e le formule che si incontrano in ogni singola tab sono ivi spiegate.

- d Densità.
- F Formula peso corrispondente alla formula stampata.
- g Quando viene posto sotto, g indica che la quantità si riferi allo stato gasoso.
- H Quando viene posto sotto, H indica che la quantità si riferi all'idrogeno, H_2.
- M Peso molecolare.
- n Indice di rifrazione riferito al vuoto.
- p Pressione.
- λ Lunghezza d'onda.
- λ_μ Valore di λ quando l'unità è $1\mu = 10^4$ Å; $\lambda_\mu = 10^{-4}\lambda_{Å}$.

The indices for solids and liquids are given for the actual temperatures at which they were determined; those for gases and vapors have in most cases been reduced to 0°C and 760 mm of Hg by some one of several, not always concordant, formulae. As values obtained previous to 1898 have been collected by Dufet (23), such values are, in general, omitted from this section if more recent data of equal or superior accuracy are available; a discussion of them will usually be found in the recent papers.

The variation of the refractivity with temperature and pressure has been given special consideration in the case of air; for other gases and vapors the available data are included with the refractivities in Table 4, if there is an indication that the ideal gas laws do not apply.

REFRACTIVITY OF AIR

Except as the contrary is stated, the following data refer to dry air containing the normal amount (0.03%) of CO_2. Doubling this amount of CO_2 will increase n by less than 1 in 10^7 (54).

TABLE 1.—REFRACTIVITY OF DRY AIR

For dispersion formulae, *see* Table 2; unit of $\lambda = 1$ Å; of $p = 1$ mm of Hg; temperature $= t$,°C

(*A*) Range: $\lambda = 2218$ to 8999, $p = 760$ mm (54). Observations were made at constant t, and gave directly the values of n for pressures near 760; these were reduced to $p = 760$ on the assumption that over this short range $(n-1)/p$ is independent of p. For smoothed values, *see* Table 3.

t	0°C	15°C	30°C
λ		$(n-1)10^8$	
2218Cu			298.27
2246Cu			296.04

REFRACTIVITY: DRY AIR.—(*Continued*)

t	0°C	15°C	30°C
λ		$(n-1)10^8$	
2303Cu			290.75
2369Cu			287.90
2392Cu	322.34	305.00	286.71
2406Cu	322.27		286.94
2411Cu	320.90	304.66	286.23
2492Cu	319.66	301.22	285.77
2618Cu	314.58	296.24	283.36
2739Fe	310.17	293.20	280.40
2766Cu	313.94	295.05	278.71
2824Cu	310.38	294.08	277.93
2851Fe	308.58		276.83
2882Cu	308.06	292.10	277.41
2918Fe	307.98	291.23	275.21
2961Cu	307.83	291.40	274.62
2987Fe	307.37	291.80	274.48
2997Cu	307.42	291.53	274.26
3010Cu	307.82	289.48	275.19
3036Cu	308.41	290.82	274.50
3055Fe		291.05	
3063Cu	306.61	290.12	275.07
3075Fe			274.73
3116Fe	304.89	288.98	274.64
3175Fe	303.43	289.40	272.02
3205Fe	303.82	288.49	272.71
3280Fe	302.89	287.25	273.25
3347Fe	302.27	285.70	272.08

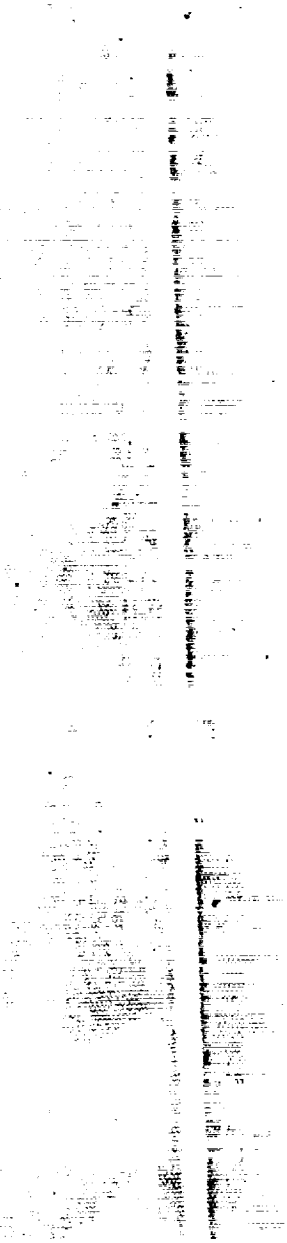

REFRACTIVITY: DRY AIR.—(*Continued*)

t	0°C	15°C	30°C
λ		$(n-1)10^8$	
3413Fe	302.36	285.97	271.56
3485Fe	300.45	285.70	
3513Fe	301.00	285.80	271.60
3594Fe	298.89	284.50	271.49
3640Fe	298.61	284.24	270.00
3659Fe	299.87	283.63	269.96
3701Fe	299.64	283.42	267.99
3753Fe	298.80	283.18	268.80
3787Fe		283.16	
3790Fe		282.91	
3843Fe	297.75	282.92	268.95
3846Fe			268.22
3865Fe		282.61	
3867Fe	298.14		
3906Fe	299.33	282.16	267.61
3935Fe	297.98	281.48	268.91
3969Fe		281.98	
3977Fe	296.62	281.59	268.14
3983Fe	297.37	282.14	267.73
4005Fe		281.75	
4021Fe	297.17	281.57	266.99
4076Fe	297.04	281.61	268.87
4095Fe	296.66	280.95	267.60
4118Fe	297.34	280.93	
4147Fe		280.78	266.68
4191Fe		280.77	
4210Fe	297.00	280.81	266.87
4213Fe	296.36	280.53	266.97
4233Fe		280.71	
4245Fe	296.59	280.47	266.80
4282Fe	295.61	280.76	265.07
4315Fe	296.08	280.04	266.38
4352Fe	296.75	280.59	266.28
4369Fe	295.42	279.61	266.30
4375Fe		279.83	
4422Fe	295.47	279.28	266.44
4427Fe		279.67	
4484Fe	295.09		
4494Fe		279.64	265.62
4531Fe		279.44	
4547Fe	294.73	278.90	265.50
4592Fe	294.34	279.19	265.49
4602Fe		279.07	
4647Fe	294.63	278.78	265.49
4691Fe	294.30	278.52	264.97
4736Fe	293.89	278.92	265.36
4789Fe	293.57	277.84	264.74
4859Fe	293.80	278.76	264.65
4903Fe	293.76	278.32	264.71
4966Fe	293.32	278.91	264.60
5001Fe	293.55		264.20
5012Fe		278.30	
5051Fe	293.59	276.40	264.20
5110Fe	293.05	278.43	264.33
5167Fe	292.68	277.93	263.90
5171Fe	293.09	277.69	263.73
5232Fe	293.42	277.92	263.64
5266Fe	293.87		263.65
5324Fe	293.61	277.59	263.08
5397Fe	293.01	277.19	263.61
5455Fe	292.44	277.34	263.43
5506Fe	292.26	277.28	263.60

REFRACTIVITY: DRY AIR.—(*Continued*)

t	0°C	15°C	30°C
λ		$(n-1)10^8$	
5569Fe	292.59	277.90	263.13
5624Fe	293.13	277.61	263.26
5658Fe	292.37	277.07	263.00
5709Fe	293.16	277.13	262.82
5763Fe	292.51	276.75	262.41
5852Ne		276.92	262.96
5881Ne		276.81	262.99
5883Fe	292.46	276.75	
5934Fe		276.71	263.88
5944Ne		276.36	262.99
6003Fe	292.85	276.58	
6029Fe			263.41
6065Fe	291.89	276.70	262.40
6074Ne		276.42	262.61
6096Ne		276.36	262.61
6136Fe	291.52	276.60	262.34
6143Ne		276.49	262.59
6163Ne		276.21	262.66
6191Fe	291.33	276.70	262.07
6217Ne		276.15	262.57
6219Fe		276.29	
6230Fe		276.79	
6246Fe		276.73	
6252Fe	291.26	276.07	262.07
6266Ne		276.49	262.48
6297Fe	290.40	274.65	
6304Ne		275.77	262.38
6318Fe		276.74	
6331Ne		276.16	262.47
6335Fe	291.06	275.81	262.10
6382Ne		276.36	262.40
6393Fe	291.11	276.37	262.03
6400Fe		276.51	
6402Ne		276.32	262.39
6430Fe	291.01	276.14	261.53
6462Fe	290.55	276.90	262.18
6494Fe	290.70	276.18	261.80
6506Ne		276.22	262.15
6532Ne		276.10	262.27
6546Fe	290.90	276.10	261.98
6563H		276.02	
6598Ne		276.02	261.96
6609Fe	291.69	276.28	261.25
6663Fe	291.36	275.96	262.74
6678Ne		275.46	
6678Fe	290.75	276.02	261.82
6717Ne		276.02	261.81
6750Fe	290.19	276.24	262.68
6752A		275.60	
6841Fe	290.70		
6843Fe			260.94
6871A		275.09	
6916Fe			263.33
6929Ne		275.76	261.84
6937A		275.45	
6945Fe	289.97	274.93	262.13
6965A		274.87	
6978Fe	290.39	275.08	261.45
7016Fe		276.54	
7023Fe	290.91		
7030A		274.90	
7032Ne		275.71	261.74

REFRACTIVITY: DRY AIR.—(*Continued*)

t	0°C	15°C	30°C
λ	$(n-1)10^6$		
7038Fe			261.01
7059Ne		273.70	
7067A		274.87	
7068Fe	290.24	276.71	262.41
7090Fe	290.53		
7130Fe	289.87	275.76	260.90
7147A		274.99	
7161Fe	289.50	276.12	261.36
7173Ne		275.67	
7187Fe		274.93	262.64
7207Fe		275.29	
7223Fe	290.57		260.89
7245Ne		275.26	261.66
7272A		274.88	
7293Fe	291.45		262.24
7372A		275.12	
7383A		274.66	
7389Fe	289.77		261.18
7411Fe	290.06	275.19	262.02
7438Ne		274.24	
7445Fe	290.36	275.62	260.94
7495Fe	290.68	276.45	261.27
7503A		274.83	
7511Fe		274.97	
7514A		274.89	
7531Fe	289.72	274.07	261.66
7568Fe			260.68
7586Fe	290.30		261.66
7620Fe		274.81	259.47
7635A		274.61	
7661Fe	289.58	274.81	261.12
7710Fe			261.12
7721A		274.49	
7748Fe	289.02	274.17	260.31
7780Fe	289.74	274.73	260.29
7832Fe	290.23	275.06	261.12
7937Fe	288.78	274.55	261.51
7945Fe	290.49	271.71	261.27
7948A		274.54	
7998Fe	288.67	274.87	260.66
8006A		274.58	
8014A		274.36	
8046Fe	289.03	275.01	260.56
8085Fe	290.26	273.92	261.00
8103A		274.28	
8115A		274.20	
8220Fe	289.52	273.61	261.22
8264A		274.25	
8327Fe	289.43	273.88	260.66
8387Fe	289.04	274.12	259.93
8408A		274.36	
8424A		274.27	
8468Fe	290.01		260.66
8514Fe		274.59	260.42
8521A		274.63	
8611Fe			259.90
8661Fe	288.10	274.07	260.10
8674Fe			261.26
8688Fe	288.73	273.41	260.18
8824Fe		273.55	260.54
8999Fe		273.56	259.15

(*B*) Values by various observers. Range: λ = 2 652 to 130 000. For older values, *see* (23, 54, 58). Data reduced by the formula

$$r_0 = r \cdot \frac{760}{p} \cdot \frac{1+\alpha t}{1+\gamma p};\ r = (n-1)10^6$$

λ	r_0
$\gamma = 0$, $\alpha = \frac{1}{273}$ (29)	
2 652	314.00
2 894	309.02
2 967	307.37
3 022	306.62
3 188	304.30
3 965	298.00
4 471	295.55
4 713	294.10
5 016	293.50
5 876	291.96
6 678	291.20
$\gamma = 0$, $\alpha = \frac{1}{273}$ (14)	
4 861	295.11
5 461	293.60
5 790	292.98
6 563	291.92

λ	r_0
$\gamma = 7(10)^{-7}$, $\alpha = 0.003670$ (35)	
5 894	292.98
67 094	288.06
86 784	288.75
$\gamma = 7(10)^{-7}$, $\alpha = 0.003670$ (75)*	
10 000	290
20 000	289
30 000	289
40 000	289

* Based on preceding value for λ = 5894, Koch (35)

λ	r_0
(62)	
5 461	293.42

λ	r_0
(81)	
5 461	291.41
(28)	
4 359	295.2
5 461	292.9
(84)	
8 000	290.9
10 000	289.7
20 000	288.2
30 000	288.5
40 000	288.0
50 000	287.9
63 000	287.3
80 000	287.8
130 000	286.9

Variation of Refractivity of Air with Temperature, Pressure and Humidity

Temperature.—$(n-1)_0 = (n-1)_t \cdot (1+\alpha t)$. Meggers and Peters (54) find $\alpha = 0.00367 + \frac{0.000003}{\lambda^2}$; Koch (35) and Statescu (75) used $\alpha = 0.003670$; Pérard (59) used $\alpha = 0.003716$; Cuthbertson (14), Howell (29), and most of the other workers have used $\alpha = 0.003663 = \frac{1}{273}$. At $t = -189$ to -188°C, Ayres (3) obtained the following values, agreeing with those of Scheel (68):

λ		507	735	914 mm of Hg
5461 Å	$(n-1)10^6 =$	651.3	951.1	1189.9
5780 Å	$(n-1)10^6 =$	653.3	951.1	1186.4

Pressure.—For small ranges in p, t constant, $(n-1)/p$ may be regarded as a constant. Opinions differ regarding the effect of relatively great changes. Mathews (53) concludes that $(n-1)/p$ is constant over the range $p = 26$ to $p = 760$ mm, but many consider that Mascart's relation, $(n-1)/p = K(1+\gamma p)$, fits the observations better; the following values have been used for γ, the unit of p being 1 mm of Hg:

λ	5 461	5 461	5 462
p	0 to 760	0 to 760	760 to 7 600
$10^8\gamma$	357 ± 39	667 ± 87	51 ± 5
Lit.	(62)	(81)	(58)
λ	4 359	4 000 to 6 500	5 000 to 86 000
p	760 to 7 600	near 760	0 to 760
$10^8\gamma$	53 ± 5	240	70
Lit.	(58)	(59)	(35)

For the range λ = 4050 to 5090 Å, $p = 30$ to 100 atm., $t = 0$ to 14°C, it has been found (70, 71, 73) that, whatever the pressure,

$$\frac{(n-1)\lambda}{(n-1)_{\lambda 5461}} = 0.08086\left\{1 + \frac{0.0056376}{\lambda^2} + \frac{54.01(10)^{-6}}{\lambda^4}\right\}$$

For variation with p at $t = -188$°C, *see* preceding text.

Humidity.—If n_d and n_m = index for dry air and for air in which the partial pressure of water vapor is m mm of Hg, then Lorenz (43) concludes that $n_d = n_m + \frac{41m(10)^{-6}}{760}$.

TABLE 2.—DISPERSION FORMULAE FOR DRY AIR

$\lambda_\mu = 10^{-4}\lambda_A$, unit of $\lambda_A = 1$ Å

For the formula $(n-1)10^6 = \beta/(\mu - \lambda_\mu^{-2})$, Cuthbertson (14) finds $\beta = 51.626$, $\mu = 179.17$; for the Cauchy formula $(n-1)\ 10^6 = A + B\lambda_\mu^{-2} + C\lambda_\mu^{-4}$, the following values have been found, those of (54) being the best. Temperature is t, °C; pressure = 760 mm of Hg, except as noted.

t, °C	A	B	C	$1000B/A$	$10^6C/A$	Lit.
0	287.566	1.3412	0.03777	4.6641	131.35	(54)
15	272.643	1.2288	0.03555	4.5070	130.39	(54)
30	258.972	1.2259	0.02576	4.7337	99.47	(54)
0	287.987*	1.804*	0	6.264*	0	(54)
0	288.02	1.482	0.0309	5.145	107.3	(65)
11				5.638†	54.01†	(59)
						(70, 71, 73)

* Freed of CO_2.

† For pressures between 30 and 100 atm., t = 12°C, 4050 Å < λ < 5090 Å.

TABLE 3.—CORRECTIONS FOR CONVERTING WAVE-LENGTHS AND THEIR RECIPROCALS IN AIR AT 15°C AND 760 MM OF HG TO THEIR VALUES IN A VACUUM (54)

If λ_a, λ_v = values in air and in vacuum, respectively, then $\lambda_v = \lambda_a + \delta_\lambda$ and $1/\lambda_a = 1/\lambda_v + \delta_\nu$, where δ_λ and δ_ν have the values given in the table. The values of $(n-1)$ are those computed by means of the equation $(n-1)10^6 = 272.643 + 1.2288\lambda_\mu^{-2} + 0.03555\lambda_\mu^{-4}$ which was derived from the observations in Table 1, section A. Unit of λ and δ_λ = 1 Å; of δ_ν = 1 cm^{-1} = 10^8 $Å^{-1}$.

λ	$(n-1)10^6$	δ_λ	δ_ν
2 000	325.582	0.6512	16.274
2 050	322.012	0.6601	15.703
2 100	318.786	0.6695	15.175
2 150	315.863	0.6791	14.687
2 200	313.207	0.6891	14.232
2 250	310.787	0.6993	13.808
2 300	308.575	0.7097	13.412
2 350	306.550	0.7204	13.041
2 400	304.691	0.7313	12.692
2 450	302.981	0.7423	12.363
2 500	301.405	0.7535	12.053
2 550	299.948	0.7649	11.759
2 600	298.600	0.7764	11.481
2 650	297.350	0.7880	11.217
2 700	296.188	0.7997	10.967
2 750	295.108	0.8115	10.728
2 800	294.100	0.8235	10.500
2 850	293.160	0.8355	10.283
2 900	292.280	0.8476	10.076
2 950	291.457	0.8598	9.877
3 000	290.685	0.8721	9.687
3 050	289.960	0.8844	9.504
3 100	289.279	0.8968	9.329
3 150	288.638	0.9092	9.160
3 200	288.033	0.9217	8.998
3 250	287.463	0.9343	8.842
3 300	286.924	0.9469	8.692
3 350	286.415	0.9595	8.547
3 400	285.933	0.9722	8.407
3 450	285.476	0.9849	8.272
3 500	285.043	0.9977	8.142
3 550	284.632	1.0104	8.016
3 600	284.241	1.0233	7.893
3 650	283.869	1.0361	7.774
3 700	283.516	1.0490	7.660
3 750	283.179	1.0619	7.550
3 800	282.858	1.0749	7.442
3 850	282.551	1.0878	7.337
3 900	282.259	1.1008	7.235
3 950	281.979	1.1138	7.137
4 000	281.712	1.1268	7.041
4 050	281.456	1.1399	6.948
4 100	281.211	1.1530	6.857
4 150	280.976	1.1661	6.769
4 200	280.751	1.1792	6.683
4 250	280.536	1.1923	6.599
4 300	280.329	1.2054	6.517
4 350	280.130	1.2186	6.437
4 400	279.939	1.2317	6.360
4 450	279.755	1.2449	6.285
4 500	279.578	1.2581	6.211
4 550	279.408	1.2713	6.139
4 600	279.244	1.2845	6.069
4 650	279.086	1.2978	6.000
4 700	278.934	1.3110	5.933
4 750	278.788	1.3242	5.868
4 800	278.646	1.3375	5.804
4 850	278.509	1.3508	5.741
4 900	278.378	1.3640	5.680
4 950	278.250	1.3773	5.620
5 000	278.127	1.3906	5.561
5 050	278.008	1.4039	5.503
5 100	277.893	1.4173	5.447
5 150	277.781	1.4306	5.392
5 200	277.674	1.4439	5.336
5 250	277.569	1.4572	5.285
5 300	277.468	1.4706	5.234
5 350	277.370	1.4839	5.183
5 400	277.275	1.4973	5.133
5 450	277.183	1.5106	5.084
5 500	277.094	1.5240	5.037
5 550	277.007	1.5374	4.990
5 600	276.923	1.5508	4.944
5 650	276.841	1.5642	4.899
5 700	276.762	1.5775	4.854
5 750	276.685	1.5909	4.811
5 800	276.610	1.6043	4.768
5 850	276.537	1.6177	4.726
5 900	276.466	1.6311	4.685
5 950	276.398	1.6446	4.644
6 000	276.331	1.6580	4.604
6 050	276.265	1.6714	4.565
6 100	276.202	1.6848	4.527
6 150	276.140	1.6983	4.489
6 200	276.080	1.7117	4.452
6 250	276.022	1.7251	4.415
6 300	275.965	1.7386	4.379
6 350	275.909	1.7520	4.341
6 400	275.855	1.7655	4.309
6 450	275.802	1.7789	4.275
6 500	275.751	1.7924	4.241
6 550	275.700	1.8058	4.208
6 600	275.651	1.8193	4.175
6 650	275.604	1.8328	4.143
6 700	275.557	1.8462	4.112
6 750	275.511	1.8597	4.081
6 800	275.467	1.8732	4.050
6 850	275.423	1.8866	4.020
6 900	275.381	1.9001	3.990

TABLE 3.—(*Continued*)

λ	$(n-1)10^6$	δ_λ	δ_p
6 950	275.339	1.9136	3.961
7 000	275.299	1.9271	3.932
7 050	275.259	1.9406	3.903
7 100	275.221	1.9541	3.875
7 150	275.183	1.9676	3.847
7 200	275.146	1.9811	3.820
7 250	275.110	1.9945	3.793
7 300	275.074	2.0080	3.767
7 350	275.039	2.0215	3.741
7 400	275.006	2.0350	3.715
7 450	274.972	2.0185	3.690
7 500	274.940	2.0620	3.665
7 550	274.908	2.0756	3.640
7 600	274.877	2.0891	3.616
7 650	274.846	2.1026	3.592
7 700	274.817	2.1161	3.568
7 750	274.788	2.1296	3.545
7 800	274.759	2.1431	3.522
7 850	274.731	2.1566	3.499
7 900	274.703	2.1702	3.476
7 950	274.676	2.1837	3.454
8 000	274.650	2.1972	3.432
8 050	274.624	2.2107	3.410
8 100	274.599	2.2243	3.389
8 150	274.574	2.2378	3.368
8 200	274.549	2.2513	3.347
8 250	274.525	2.2648	3.326
8 300	274.502	2.2784	3.306
8 350	274.478	2.2919	3.286
8 400	274.456	2.3054	3.266
8 450	274.434	2.3190	3.246
8 500	274.412	2.3325	3.227
8 550	274.390	2.3460	3.208
8 600	274.369	2.3596	3.189
8 650	274.349	2.3731	3.170
8 700	274.328	2.3867	3.152
8 750	274.309	2.4002	3.134
8 800	274.289	2.4137	3.116
8 850	274.270	2.4273	3.099
8 900	274.251	2.4408	3.080
8 950	274.232	2.4544	3.063
9 000	274.214	2.4679	3.046
9 050	274.196	2.4815	3.029
9 100	274.179	2.4950	3.012
9 150	274.161	2.5086	2.995
9 200	274.144	2.5221	2.979
9 250	274.128	2.5357	2.963
9 300	274.111	2.5492	2.947
9 350	274.095	2.5628	2.931
9 400	274.079	2.5763	2.915
9 450	274.064	2.5899	2.899
9 500	274.048	2.6035	2.881
9 550	274.033	2.6170	2.869
9 600	274.018	2.6306	2.854
9 650	274.004	2.6441	2.839
9 700	273.989	2.6577	2.824
9 750	273.975	2.6713	2.809
9 800	273.961	2.6848	2.795
9 850	273.947	2.6984	2.780
9 900	273.934	2.7119	2.766
9 950	273.920	2.7255	2.752
10 000	273.907	2.7391	2.738

TABLE 4.—REFRACTIVITY OF GASES AND VAPORS

For dispersion formulae, *see* Table 5

Order: Elementary substances, pure compounds, mixtures. The formula used for reducing the observations is indicated, if known, by *I*, *II*, or *III*: *I*, $r_0 = r\cdot\frac{760(1+\alpha t)}{p(1+\gamma p)}$, unless other values are given, $\gamma = 0$ and $\alpha = 1/273$; *II*, $r_0 = rd_0/d$; *III*, $r_0 = r[(F/d)_0]_{t,p} \times [(d/M)_n]_{0,760}$; $r = (n-1)10^6$. If the gas is ideal and diatomic, and if $\gamma = 0$ and $\alpha = 1/273 (= 0.003663)$, all three formulae give the same value, and $r_0 = 10^6(n-1)_{0,760}$. $K = r_0/p$. Unit of $\lambda = 1$ Å; of $p = 1$ mm of Hg; temperature $= t$,°C.

I. Å-Table.—Elementary Substances

A, Argon; *cf.* (82)*

λ	r_0
I (65)	
2 441.6	303.78
2 492.1	302.80
2 618.4	300.38
2 766.1	298.11
2 824.4	297.14
2 961.2	295.50
3 319.3	291.62
4 275.1	286.34
4 651.1	284.99
5 105.6	283.79
5 153.2	283.67
5 218.2	283.50
5 700.2	282.55
5 782.2	282.47
III (16); *cf.* (12)	
4 800	283.8
5 086	283.1
5 209	282.8
5 461	282.3
5 769	281.7
5 790	281.7
6 438	280.9
(7)	
4 861	286.0
5 016	285.6
5 461	284.6
5 876	283.8
5 896	283.7
6 563	282.9
(1)†	
4 359	285.1
5 461	281.6
5 770	280.2
5 790	280.2
6 439	279.6

* At 0°C and 760 mm Hg, (82) finds $r_0 = 282.70$ for $\lambda = 5462.3$.

† Less accurate than those of (16).

As₂, Arsenic

III (20)

5 461	1 579
5 893	1 552

Br₂, Bromine

III (18)

5 461	1 184.9
5 600	1 179.6
5 700	1 176.2
5 750	1 174.1
5 800	1 173.5
6 000	1 166.2

Br₂.—(*Continued*)

λ	r_0
6 438	1 157.0
6 708	1 152.5

Cd₂, Cadmium

III (20)

5 183	2 780
5 461	2 725
5 893	2 675
6 562	2 675

Cl₂, Chlorine

III (18)

4 799.9	791.66
5 085.8	787.91
5 209.1	786.51
5 460.7	784.00
5 769.5	781.35
5 790.5	781.21
6 438.5	777.03
6 707.85	775.63

F₂, Fluorine

III (21)

5 893	195 *ca.*

H₂, Hydrogen*

I (14)

4 861	140.64
5 461	139.71
5 780	139.33
6 563	138.66
I (35, 36); *cf.* (34)	
2 303	159.435
2 379	157.693
2 448	156.300
2 465	155.978
2 536	154.604
2 577	154.017
2 676	152.538
2 754	151.510
2 761	151.423
2 858	150.268
2 891	149.873
2 926	149.530
2 968	149.118
3 127	147.717
3 133	147.661
3 342	146.130
3 545	144.950
3 664	144.321
3 705	144.103
3 908	143.246
3 985	142.979

H_2.—(*Continued*)

λ	r_0
4 048	142.749
4 079	142.642
4 109	142.550
4 360	141.785
4 917	140.527
5 462	139.660
5 895	139.24
6 710	138.53
67 091	136.10
86 784	136.06

(43)

5 896	138.7
6 708	138.0

I (48)

$\gamma = 0$, $\alpha = 0.00381$

5 085	130.2
5 896	136.7
6 438	136.3

(60)

4 677	140.8
4 800	140.6
5 085	140.0
5 378	139.3
5 896	139.0
6 438	138.5

I (68)

4 358	140.6
4 712	139.8
4 922	139.6
5 780	138.9
6 676	137.6

I (29)

2 753	151.87
2 894	150.61
3 022	149.73
3 341	147.37
4 026	144.40
4 471	142.80
4 713	142.38
4 916	142.03
5 876	141.05

I (33)

1 854.6	175.996
1 862.7	175.541
1 935.8	171.824
1 990.5	169.395
2 303	159.418
2 379	157.681
2 536	154.690
2 754	151.500
2 894	149.859
2 968	149.101
3 342	146.133
4 048	142.741
4 079	142 632
4 360	141.773
5 461	139.650†

* For the range $56 < p < 2760$ mm of Hg and t = constant, $(n-1)10^6 = kp$, even at very low temperatures; for $\lambda = 5461$, $k = 0.615$ if $t = -187.5$°C, and $k = 0.687$ if $t = -191.1$°C; for $\lambda = 5780$, $t = -191.1$°C, $k = 0.683$ per mm of Hg (3).

† Same value found by Schacherl (67).

He, Helium; *cf.* (82)

λ	r_0
III (16)	
4 800	35.04
5 086	34.99
5 209	34.98
5 461	34.95
5 769	34.82
5 791	34.92
6 438	34.86
I (37)	
2 303	36.258
2 379	36.146
2 448	36.063
2 465	36.046
2 536	35.959
2 577	35.916
2 676	35.827
2 754	35.760
2 761	35.749
2 858	35.672
2 894	35.646
2 926	35.624
2 968	35.605
3 342	35.396
3 515	35.133
3 861	35.197
3 985	35.173
4 109	35.139
4 917	34.989
5 462	34.925
I (7)	
4 861	35.10
5 016	35.08
5 461	35.04
5 876	35.00
5 896	35.00
6 563	34.95

Hg_2, Mercury

III (20)

5 183	1 885
5 461	1 882
5 893	1 866
6 562	1 799

I_2, Iodine*

III (18)

5 000	$2\ 12_0$
5 005	$2\ 16_0$
5 100	$2\ 21_0$
5 250	$2\ 25_0$
5 600	$2\ 17_0$
6 180	$2\ 13_0$
6 215	$2\ 13_0$
6 438	$2\ 10_0$
6 708	$1\ 97_0$

* Not very accurate.

K, Potassium*

* For dispersion near absorption bands, *see* Bevan (5).

Kr, Krypton

III (16)

4 799.9	431.80
5 085.8	430.34
5 029.1	429.78
5 460.7	428.74
5 769.5	427.64

Kr.—(*Continued*)

λ	r_0
5 790.5	427.61
6 438.5	425.80
6 707.8	425.33

N_2, Nitrogen;* *cf.* (83)

I (14)

4 861	301.21
5 461	299.77
6 563	298.16

I (37)

$\alpha = 0.003675$

2 379	326.09
2 448	324.11
2 465	323.61
2 536	321.80
2 577	320.84
2 676	318.71
2 754	317.21
2 760	317.08
2 858	315.42
2 894	314.81
2 926	314.34
2 968	313.74
3 342	309.37
3 515	307.64
3 705	306.36
3 908	305.11
3 985	304.73
4 079	304.24
4 109	304.06
4 917	301.06
5 461	299.77

I (68)

$\alpha = 0.003675$

4 358	302.0
4 712	301.4
4 922	299.9
5 461	298.2
5 780	297.6
6 576	296.1
7 056	294.5
I (66)	
3 342	307.0
3 650	303.4
4 046	301.0
4 358	299.5
5 461	296.7
5 769	296.6

(3)

$t = -189.2$°C; $\lambda = 5461$ Å

$\Delta\ddagger = 0.036p$

p†	$(n-1)10^6$
10.1 cm	133.3
21.9	288.2
35.5	461.8
42.8	558.9
76.2	1 004.0
76.4	1 009.9
76.6	1 008.6
100.9	1 347.0
101.0	1 349.3
122.8	1 662.5
122.8	1 659.0
143.4	1 961.1
143.5	1 962.9
149.5	2 049.7

N_2.—(*Continued*)

$t = -190.6$°C; $\lambda = 5461$ Å

$\Delta\ddagger = 0.035p$

p†	$(n-1)10^6$
10.8 cm	144.1
22.2	294.4
35.6	470.6
39.0	515.3
72.6	975.4
76.3	1 023.3
110.4	1 508.3
123.3	1 692.4
132 3	1 829.9

$t = -191.6$°C; $\lambda = 5461$ Å

$\Delta\ddagger = 0.23p$

11.0 cm	149.8
20.2	278.5
33.9	456.6
75.8	1 034.3
119.6	1 669.5

* At 21°C, $\lambda = 5461$ Å, and d between $70d_0$ and $200d_0$. d_0 = density at 0°C and 760 mm, $\frac{n^2-1}{n^2+2}\cdot\frac{d_0}{d}$ ($= 199.7 \times 10^{-6}$) is more nearly constant than either $(n^2-1)/d$ or $(n-1)/d$ (57).

† If computed by van der Waals's equation with $a = 126\,070$, $b = 1.325$, then both $(n-1)/d$ and $(n^2-1)/(n^2+2)d$ are constant within 2 c%.

‡ $\Delta = (n_{5461} - n_{5780}) \times 10^6$, where 5780 is the mean λ of the yellow lines of Hg; p is expressed in cm of Hg. At -191.6°C the coefficient of p is nearly 7 times as great at -190.6°C.

Na, Sodium*

* For dispersion near absorption bands, *see* Bevan (5).

Ne, Neon

III (16)

4 799.9	67.31
5 085.8	67.23
5 209.1	67.21
5 460.7	67.16
5 769.5	67.10
5 790.5	67.10
6 438.5	67.02

O_2, Oxygen*

I (14)

4 861	273.45
5 461	271.70
5 790	270.99
6 563	269.75
I (29)	
2 753	321.23
2 894	293.60
3 022	291.19
3 188	287.93
3 889	279.65
4 471	276.31
4 713	275.11
5 016	274.01
5 876	271.84
6 678	270.83

551.5 Sm5

531.9 Sm5